On the importance of temperature and precipitation changes for glacial ice sheet stability

Ning Zhou

Master's thesis in geosciences

Department of Earth Science

University of Bergen

November 20, 2023

Abstract

Ice sheets undergo periodic advances and retreats, resulting in glacial-interglacial cycles. The Last Glacial Period is widely believed as involving a long-time buildup phase followed by a rapid termination over approximately 100 thousand years (kyr), resulting in a characteristic sawtooth pattern. This pattern aligns with the dominant 100-kyr cycle observed over the past million years. While there is a consensus on the significance of temperature and moisture contents as crucial factors in initiating and terminating glaciations, the precise role of these factors in governing glacial inceptions and terminations remains largely elusive. In this study, we assess the relative significance of temperature and precipitation anomalies during key glacial periods. We find as glacial severity intensifies, precipitation anomalies gain significance, yet temperature anomalies remain the primary influencer of Surface Mass Balance (SMB) variations. Our findings suggest that temperature anomalies may play a pivotal role in both glaciation inception and termination. However, it is important to note that this conclusion is drawn from the present day-LGM anomaly of a single climate model. If the magnitude difference between temperature anomalies (°C) and precipitation anomalies (mm/day) is less pronounced, the influence of precipitation could become more prominent.

Acknowledgements

As an untypical student, embarking on a master's program in a relatively new field was a challenge, yet it turns out to be an enjoyable and incredibly rewarding journey with the completion of this thesis.

First and foremost, I would like to express my deepest gratitude to my main supervisor Prof. Andreas Born for the invaluable guidance, support, and encouragement throughout the research process. Many thanks for designing this interesting master project, helping me build the fundamental understanding of the subject, helping me solve all the problems I meet and giving me the insightful feedbacks weekly, which makes it possible to advance and shape this thesis finally. Thank you for your expertise and leading me to discover the beauty of the numerical modelling. It has been a great pleasure to be under your supervision.

I am also immensely grateful to Rebekka Frøystad for the exceptional assistance and patience throughout this process. Thank you for instructing me to use the basic tools for this study, which provides me the foundation for the further work, and thank you for addressing all my queries and always being supportive.

I want to further extend my sincere thanks to all the teachers and courses that significantly enrich my knowledge in paleoclimate and glaciology through this wonderful journey. I also want to thank UiB and the administration for offering me this opportunity to experience this rewarding academic pursuit.

Finally, I am deeply indebted to my family for the tremendous love, care, and support. Thank all my family members for being my rock, making my life complete, and motivating me to take on challenges. I also want to thank my resilient friends, reminding me that despite life's challenges, there's always a bright side to strive for.

Ning Zhou

Bergen, November 2023

Contents

List of Figures

Chapter 1

Introduction

Ice sheets hold both practical and scientific significance due to their profound impact on climate and sea level. They play a crucial role in Earth's climate system by altering the surface albedo, contributing freshwater into the ocean, and influencing topography (Vizcaino, 2014). Furthermore, changes in the size of ice sheets have significant impacts on sea level. Understanding the complex interaction between ice sheets and climate system is essential for predicting future climate changes and sea level rise, while also presenting an intellectual challenge.

Ice sheets interact with various components of the Earth's system, including the atmosphere, ocean, and solid Earth (Goelzer et al., 2017). Studies suggest that surface processes interacting with the atmosphere predominantly control the total ice volume change for most glaciers and ice sheets. This is especially evident on Greenland, where considerable mass losses are occuring (Ettema et al., 2009; van den Broeke et al., 2017). Thus, surface Mass Balance (SMB), the net mass gain or loss from surface mass exchange, is a crucial component of comprehensive ice sheet studies. In this study, we mainly focus on the Last Glacial Period.

Glacier growth during the Last Glacial Period began in a climate that was relatively warm, similar to present day (Kukla et al., 2002; McManus et al., 2002; Miller and de Vernal, 1992). The termination phase, in contrast, began at the Last Glacial Maximum (LGM), a time characterized by an extremely cold and dry climate. The glacial initiation and termination may be attributed to the intricate nonlinear response of ice sheets to climate variations. However, the exact mechanisms governing these processes remain largely elusive, and the stability of large ice sheets remains a subject of ongoing research.

The LGM is relatively well-reconstructed and serves as a crucial reference point for exploring the intricate interactions among climate, ice dynamics and geological processes on

Earth. It stands as a pivotal point, signifying the shift from extensive glaciation to the onset of deglaciation within the Last Glacial Period. Abundant accessible geological and paleoclimatic archives from this period have greatly contributed to a relatively comprehensive understanding of this time. Generally, the LGM is characterized as colder and drier in comparison to the contemporary climate, and during this period, sea level was approximately 125 meter lower than it is today. It is widely believed that the Northern Hemisphere ice sheets underwent a long-time buildup lasting about 90 thousand years (kyr) until reaching their maximum extent during the LGM. This followed by a relatively rapid termination phase of about 10 kyr, resulting in a characteristic sawtooth pattern (Broecker and Van Donk, 1970). This 100-kyr cycle corresponds to the dominant frequency observed over the past million years. While there is a consensus on the significance of temperature and moisture contents as crucial factors in initiating and terminating glaciations (e.g., Haug et al., 2005), the precise influence of these two factors in governing glacial inceptions and terminations remains largely elusive.

Many studies have emphasized the strong link between insolation and ice volume (e.g., Hays et al., 1976; Huybers, 2011; Lisiecki, 2010). As temperature is directly affected by insolation changes, thus, it is suggested that temperature anomalies are the primary drivers for glacial inception and termination. Localized low temperatures are essential for the survival of snow cover through the summer melt, laying the foundation for new ice sheets (Gildor, 2003). However, for small glaciers to evolve into massive ice sheets, relative warm temperatures that can hold more moisture content are necessary (Gildor, 2003). Therefore, the optimal conditions for the onset of glaciation involve lower temperatures in summer coupled with higher temperatures in winter (Miller and de Vernal, 1992). Additionally, oceans contribute significantly to ice sheet growth by supplying substantial moisture (Charles et al., 1994; Lambeck et al., 2002). Thus, warm oceans are another ideal condition for the initiation of glaciation (Miller and de Vernal, 1992).

Another perspective highlights the significance of moisture content for glacial inception and termination. For instance, the onset of glaciation is attributed to an enhanced Atlantic Meridional Overturning Circulation (AMOC) that intensifies storminess and moisture transport, facilitating ice sheet growth, but not a reduced AMOC that provides less heat to high latitudes, leading to lower temperatures (Risebrobakken et al., 2007). Moreover, an alternative perspective proposes that the termination is promoted by a lack of moisture, resulting in large ice sheets being unable to maintain their original size due to insufficient moisture supply. The

temperature-precipitation feedback further facilitates the onset of deglaciation into a rapid and irreversible retreat.

In this study, we employ the surface energy and mass balance model (BESSI) to evaluate the SMB sensitivity to key variable changes. BESSI provides insights into the real sources associated with changes in SMB, grounded in physical first principles (Born et al., 2019). The climate forcing data is obtained by using two snapshots representing present-day climate and the LGM climate, respectively. The present-day climate forcing is sourced from the ERA5 reanalysis dataset, while the LGM climate forcing is derived from the Community Climate System Model, version 4 (CCSM4). A weighting factor (η) serves as a glacial-severity index, used to scale climate anomalies from present day to full glacial conditions and beyond. This study utilizes daily transient climate forcing, which is considered as an optimal choice for the surface mass balance model (Zolles and Born, 2022).

Through this study, we aim to evaluate the relative significance of temperature and precipitation anomalies during key glacial periods. By assessing the SMB sensitivity to the changes in these variables with increasing glacial severity, the dominance of temperature anomalies in driving SMB variations is evident. It is most prominent when glacial severity approaches present-day levels. As glacial severity intensifies, precipitation gains significance, but temperature anomalies continue to exert the primary influence on SMB variations, even under full glacial conditions. Our findings thus suggest that anomalies in temperature may be the dominant driver for both glaciation inception and termination.

Chapter 2

Theoretical background

2.1 Interactions between ice sheets and other Earth system components

Ice sheets are of great scientific interest due to their active interactions with other components of the Earth system. They possess the potential to influence both local and global climate through various mechanisms, including changes in freshwater input to the ocean (Bintanja et al., 2013; Broecker et al., 1988; Fichefet et al., 2003; Manabe and Stouffer, 1995; Straneo et al., 2011), alterations in topography (Gallée et al., 1992; Junge et al., 2005; Manabe and Broccoli, 1985), and variations in albedo (Box et al., 2012; Pritchard et al., 2008; van den Broeke et al., 2008). Furthermore, it is widely acknowledged that sea-level changes are primarily driven by fluctuations of ice sheets. Consequently, projecting future sea-level rise and climate change cannot be achieved without a comprehensive understanding of ice sheet dynamics. Additionally, delving into the complex interactions between the ice sheets and the climate system can enhance our knowledge of the paleoclimate evolution (Vizcaino, 2014).

Ice sheets interact with the atmosphere, ocean and solid Earth (Goelzer et al., 2017). The mass balance of an ice sheet can be expressed as:

$$MB = SMB - OMB - BMB \tag{2.1}$$

where MB denotes the total mass balance, SMB represents the overall mass gain or loss occurring at the surface, OMB signifies the mass discharge to the ocean from marine-terminating outlet glaciers (e.g., ocean melt of floating ice, iceberg calving), and BMB indicates mass loss

due to bottom melt, primarily driven by geothermal heat flux (Vizcaino, 2014).

Studies suggest that Surface Mass Balance (SMB) has the most substantial impact on changing ice volume, particularly on Greenland (Ettema et al., 2009). Consequently, active research efforts are concentrated on understanding surface processes. One of the most remarkable advancements in modelling has been the shift from empirical temperature index models to more sophisticated energy-balance models. However, challenges persist in accurately simulating SMB. One of the prominent issues is the significant discrepancy of the spatial and temporal resolutions between meteorological data and ice sheet models (Born et al., 2019).

The interaction with ocean water is another crucial forcing mechanism for ice sheets (Vizcaino, 2014). Ice sheets lose mass primarily through submarine melting and calving. OMB constitutes the largest mass loss in Antarctica (Rignot et al., 2013) and is a primary driver of ice flow acceleration in both Greenland (Holland et al., 2008) and Antarctica (Pritchard et al., 2012). Nevertheless, modelling such interaction remains challenging due to the scarcity of observational data in these inaccessible regions (Vizcaino, 2014). Despite these challenges, advances have been made in reproducing oceanic process, such as plume models (Straneo et al., 2011) and high-resolution regional models (Rignot et al., 2012).

The interaction with solid Earth generates a minor contribution to the total mass balance (van den Broeke et al., 2009) but exerts a significant influence on ice flow (Schoof, 2010). Geothermal heat flux commonly serves as a lower boundary condition and has a considerable impact on basal temperature, sliding and hydrology (Vizcaino, 2014). Despite the limited knowledge of basal conditions beneath ice sheets, significant advances have been made through the refinement of various techniques, including remote sensing and data assimilation (Vizcaino, 2014).

2.2 Surface Mass Balance (SMB)

It has been suggested that surface mass exchange plays a dominant role in controlling the total mass balance for most glaciers and ice sheets (Cuffey and Paterson, 2010). This is particularly evident in Greenland, where significant mass losses are currently taking place, significantly contributing to sea-level rise (van den Broeke et al., 2017).

SMB is the net mass gain or loss at the surface:

$$SMB = PR - RU - SU \tag{2.2}$$

where PR represents total precipitation, which is the sum of snowfall and rainfall. RU stands for the net runoff, accounting for the inflow of water (melt water and rainfall) minus the outflow of water (refrozen water), and SU represents sublimation (Vizcaino, 2014).

2.2.1 Surface Accumulation Processes

Surface accumulation depends on several factors. It is primarily controlled by the amount of snowfall, which provides a good estimate of total accumulation for mid-latitude and sub-polar glaciers. However, in polar regions, the significance of refreezing cannot be overlooked (Cuffey and Paterson, 2010). Redistribution by wind and avalanches also affects accumulation to a certain extent, which makes surface accumulation different from the simple process of snowfall. Deposition from frost and rime is typically negligible (Cuffey and Paterson, 2010), but can become important in extremely dry climates, such as the present-day Antarctica (van Wessem et al., 2018).

Snowfall

Snowfall, as the dominant factor influencing surface accumulation, varies significantly across different regions, ranging from several meters per year to just a few centimeters per year. The rate of snowfall is primarily determined by temperature. Snowfall occurs when near-surface temperatures are below the freezing point, preventing precipitation from falling as rain. Atmospheric moisture content increases exponentially with air temperature, following the Clausius-Clapeyron equation (Cuffey and Paterson, 2010):

$$E_{sw} = 2.38 \times 10^{11} \exp(-5400/T_a) \tag{2.3}$$

$$E_{si} = 3.69 \times 10^{12} \exp(-6150/T_a) \tag{2.4}$$

where E_{sw} and E_{si} are the vapor pressure at saturation (in Pa) over liquid water and ice, respectively, and T_a is the air temperature (in K).

For more precise expressions for saturation vapor pressure, please refer to Flatau et al.

(1992). On a rough estimate, a 10 °C rise in temperature can result in the doubling of the moisture content, leading to higher snowfall rates in regions with intermediate temperature conditions. In such areas, snowfall is not sharply limited by low vapor content, nor does it convert into rainfall due to excessively high temperatures.

Apart from temperature, there are several other factors influencing snowfall rates. Cooling is an essential process in precipitation formation, often resulting from the uplift of air masses due to orographic lifting, frontal systems or convective storms. Therefore, windward slopes of steep coastal mountain ranges receive abundant snowfall. Recent studies have consistently revealed a correlation between the shifting of storm tracks and variations in mass balance (Bitz and Battisti, 1999; Box et al., 2013; Nesje et al., 2000; Rasmussen and Conway, 2004). Furthermore, altitude plays a significant role in influencing snowfall rates. At higher elevations, precipitation rates tend to rise within the initial few kilometers above sea level but decrease beyond a certain threshold due to reduced moisture content (Cuffey and Paterson, 2010). This phenomenon ultimately results in an elevation-induced arid effect on polar ice sheets.

Refreezing

Refreezing denotes the freezing of previously melted snow or rain within the porous snow matrix. Although it is generally insignificant in mid-latitude and sub-polar glaciers, it holds great importance in polar regions. Previous studies indicate that about 7% of meltwater refreezes on glaciers in Iceland and Norway (Jóhannesson et al., 1995). In contrast, approximately 40% of total meltwater undergoes refreezing in Greenland (Van Angelen et al., 2013; Vizcaíno et al., 2013). Furthermore, in Antarctica, most meltwater experiences refreezing under current conditions (Lenaerts et al., 2012b).

Refreezing can occur both on the surface and internally and depends on the temperature of snow layers and the availability of pore space (Vizcaino, 2014) . The capacity for refreezing diminishes under warmer conditions due to higher snow layer temperatures and reduced pore capacity (Van Angelen et al., 2013; van den Broeke et al., 2009; Vizcaíno et al., 2013) .

Wind-borne redistribution and avalanches

While redistribution has a relatively minor impact on the overall mass balance (Das et al., 2013), it is of significance in comprehending the spatial and temporal variations in accumulation and local surface balance (Lenaerts et al., 2012a). The wind-induced process can lead

to wind scour or deposition across various regions. Additionally, avalanches serve as a crucial snow source for certain mountain glaciers (Cuffey and Paterson, 2010), but are of less importance on Greenland.

2.2.2 Surface Ablation Processes

Surface ablation processes primarily involve melt and sublimation. Sublimation has the potential to diminish the energy available for melting (Cuffey and Paterson, 2010), thereby inhibiting melting even when air temperatures are above the freezing point (Kuhn, 1987).

Surface melt

Surface melt is primarily governed by the surface energy balance. when the surface temperature rises to the melting point, any excess energy is utilized to melt snow (Born et al., 2019). The net energy flux (E_N) into the surface is expressed as follows:

$$E_N = E_R + E_S + E_L + E_G + E_P \tag{2.5}$$

where E_R represents the net radiation, E_S and E_L correspond to sensible heat flux and latent heat flux, respectively (these are also referred to as turbulent heat fluxes due to the turbulent mixing of air at the surface). E_G denotes the subsurface heat flux, E_P stands for the heat flux supplied by precipitation due to its temperature difference with the surface (Hock, 2005).

It is noteworthy that radiation (E_R) is the most significant source of surface energy flux (E_N) (van den Broeke et al., 2008; Van den Broeke et al., 2008) , followed by sensible heat flux (E_S), while latent heat flux (E_L) plays a minor role (Hock, 2005). Typically, E_P and E_G are considered negligible (Cuffey and Paterson, 2010).

Net radiation (E_R) consists of the sum of shortwave (Q_{SW}) and longwave radiations (Q_{LW}):

$$E_R = Q_{SW} + Q_{LW} \tag{2.6}$$

Direct in-situ data for net radiation are limited, thus parameterizing these components is crucial (Hock, 2005):

$$Q_{SW} = (1 - \alpha_{snow}) S_{BOA} \tag{2.7}$$

$$Q_{LW} = \sigma(\varepsilon_{air} T_{air}^4 - \varepsilon_{snow} T_{snow}^4) \tag{2.8}$$

where α_{snow} represents snow albedo, S_{BOA} is the incoming shortwave radiation at the bottom of the atmosphere, σ is the Stefan-Boltzmann constant, ε_{air} and ε_{snow} represent the emissivity of air and snow, respectively, and T_{air} and T_{snow} represent the corresponding temperatures.

Sublimation

Sublimation is more pronounced in cold conditions, particularly in polar regions. This is primarily due to the characteristics of the cold environment, where low temperature and low saturation vapor pressure actively promote this process. Consequently, sublimation plays an important role in the surface mass balance, contributing to the mass loss of ice sheets. Recent studies have consistently shown that sublimation is the predominant contributor to the surface mass loss in Antarctica (Lenaerts et al., 2012a,b), making up over 90% of the ablation over the scour zone (Das et al., 2015). In Greenland, sublimation contributes to roughly 5% of the total accumulation (Dietrich et al., 2023). Notably, in central Greenland, sublimation can account for as high as 12% - 23% (Box and Steffen, 2001).

Wind plays a significant role in promoting sublimation through various mechanisms. Wind enhances diffusion, turbulence and heat transfer, removing saturated air and replacing it with fresh, relatively dry air. These mechanisms collectively accelerate the rate of sublimation, particularly in polar regions where windy conditions are prevalent.

2.2.3 Challenges in modelling Surface Mass Balance

As surface mass balance (SMB) dominants the overall mass balance, the boundary condition of SMB is crucial for realistic ice sheet modelling (Fyke et al., 2014; Helsen et al., 2017; Vizcaino et al., 2015). Therefore, accurately calculating SMB is a prerequisite for comprehensive ice sheet studies. However, significant challenges still exist in achieving accurate SMB modelling.

Realistic modelling of SMB demands realistic climatology, explicit simulation of snow processes, and adequate horizontal resolution (Vizcaino, 2014). Despite notable progress, climate biases and insufficient resolution still pose substantial difficulties in accurately simulating climate-SMB interaction.

Previous studies have highlighted that albedo-SMB feedback is one major climate-SMB feedback mechanism (e.g., Box et al., 2012). Fresh-snow albedo decreases with aging or impurities (Box et al., 2012)), dropping from around 0.9 for fresh snow to approximately 0.7 for wet snow. When the snow melts, albedo can further decline to around 0.3 where ice is

exposed (Vizcaino, 2014). SMB models lacking explicit albedo evolution are prone to SMB biases. However, challenges persist in reconstructing reliable albedo evolution. While in-situ information on albedo has been greatly improved with the help of remote-sensing devices, a significant gap remains due to the lack of corresponding observational data concerning ice melt volume, which is closely linked to SMB. This gap poses the greatest difficulty in validating the modelled SMB.

Another critical climate-SMB feedback is the elevation-SMB feedback, as indicated by a prior study which suggested that employing a fixed topography could introduce an SMB bias of approximately 10% in Greenland (Edwards et al., 2013). High horizontal resolution is essential to represent elevation-related SMB change. Various approaches have been adopted to bridge the gap in horizontal resolution between climate models and ice sheet models while maintaining sufficient computational efficiency.

Realistic SMB simulations also rely on accurate information regarding precipitation and refreezing (van den Broeke et al., 2009). Reliable precipitation modelling relies on correct reconstructions of atmospheric circulation, orographic forcing, and the surrounding sea ice (Vizcaino, 2014).

Lastly, observational data, particularly improved spatial coverage of in-situ SMB data is urgently needed to enhance the reliability of SMB simulations (Vizcaino, 2014).

2.3 The Last Glacial Maximum (LGM)

The Last Glacial Maximum (LGM) stands as a pivotal moment in Earth's climatic history, signifying the transition from extensive glaciation to the onset of deglaciation. This epoch has attracted considerable research attention due to that it occurred relatively late in geological time. The abundance of accessible geological and paleoclimatic archives from LGM facilitates a relatively good understanding of this period, and the pronounced changes within these proxies further ensure a relatively high degree of accuracy. Additionally, its proximity to present allows for the application of a wide range of radiometric dating techniques.

LGM serves as a critical reference point for studying the intricate interactions between climate, ice dynamics and geological processes on Earth. It offers valuable insight into how Earth's climate system responds to external forcing and internal feedback mechanisms, thereby improving our capacity to predict future climate change.

2.3.1 Overview

Ice sheet reconstruction

Northern Hemisphere ice sheets reached their maximum extent during the Last Glacial Maximum (LGM), approximately 19,000 to 26,000 years ago. The variability in the estimated timing arises from the fact that different ice sheets reached their maximum extent at distinct times, and the peak cooling of climate did not align precisely with the maximum ice volume.

Ice sheet reconstruction typically relies on two primary approaches: the interpretation of geological evidence and numerical modelling (Kleman et al., 2010). However, owing to the uncertainties in age determination and limited resolution, the evolution of North American and Eurasian ice sheets during the Last Glacial Period remains largely elusive (Clark et al., 1993; Kleman et al., 2010). Nevertheless, there is a consensus that the North American ice sheet underwent a significant expansion from its initial phase to the LGM (Clark et al., 1993; Kleman et al., 2013). In contrast, Eurasian ice sheet displayed a different pattern, showing limited expansion but a pronounced westward migration, moving from northeastern Siberia toward Europe (Kleman et al., 2013; Svendsen et al., 2004) (Figure 2.1). Furthermore, the Eurasian ice sheet exhibited strong variation in its ice volume, possibly forming and melting away multiple times throughout the Last Glacial Period. For instance, the Eurasia ice sheet may have completely melted away during Marine Isotope Stage (MIS) 3, whereas the North American ice sheet experienced little melting during the same period and underwent substantial expansion from MIS 3 to MIS 2 (Mangerud et al., 2023).

Climate reconstruction

LGM was characterized by a significant global cooling. Figure 2.2 shows the spatial distribution of the LGM cooling, reconstructed through data assimilation. The global mean sea surface temperature is estimated to have been 3.1°C lower than today (Figure 2.2**c**), with particularly pronounced cooling of 8°C in the north Pacific and Atlantic regions (Figure 2.2**a**) (Tierney et al., 2020). Furthermore, the global mean surface air temperature is estimated to have been 6.1°C lower than today (Figure 2.2**d**), with substantial cooling over the places where once covered by ice sheets (Figure 2.2**b**) (Tierney et al., 2020).

Generally, the LGM is believed to have been characterized by drier and windier conditions compared to the present climate. Dust transport and accumulation were greater during

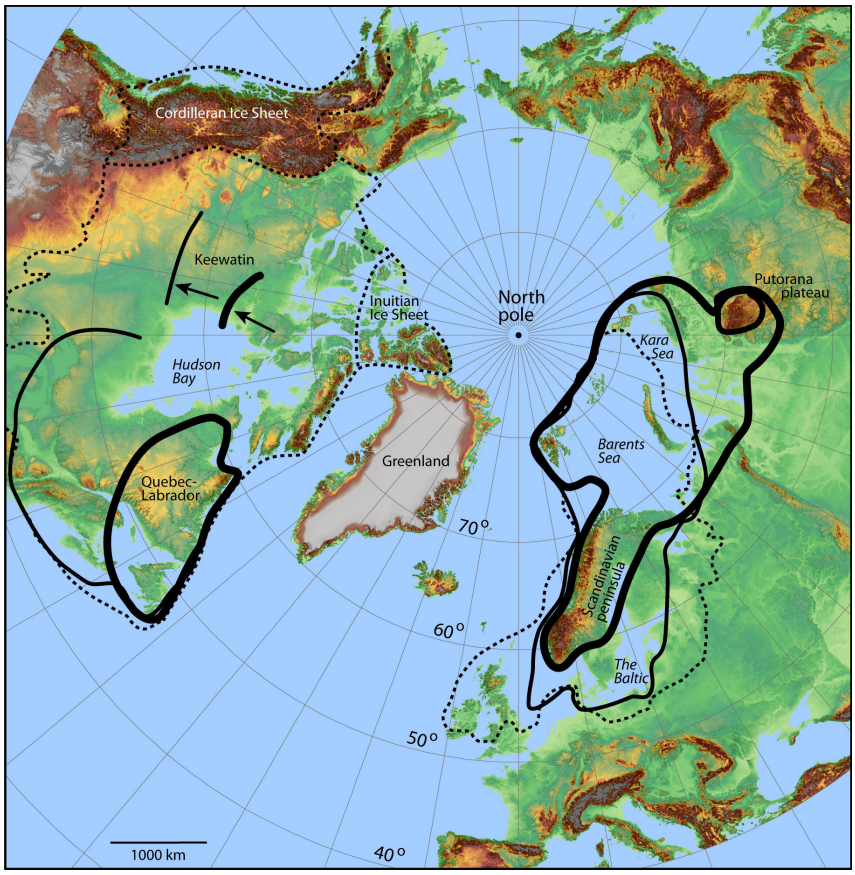

Figure 2.1: The extent of North American and Eurasian ice sheet during the Last Glacial Period. The dotted line signifies the ice-sheet extent during the LGM, while the bold and thin solid line indicate the ice margin outlines for Marine Isotope Stage (MIS) 5b and MIS 4, respectively. Figure from Kleman et al. (2013).

LGM (Sarnthein, 1978). Notable changes in precipitation patterns were observed in different regions. In North America, the southwestern USA is thought to have experienced wetter conditions, whereas the Pacific Northwest was drier during the LGM (Smith and Street-Perrott, 1983). Europe also underwent significant changes during this period. Figure 2.3 illustrates a comparison between modern vegetation and LGM vegetation. In northern Europe, forests were replaced by tundra, indicating a colder and drier climate. Conversely, around the Mediterranean, dry scrub transformed into forest, indicating a wetter climate (Flint, 1971).

Sea-level records imply valuable information about climate change. Figure 2.4 presents a sea-level reconstruction for LGM. Generally, the global sea level is estimated to have been approximately 125 meters lower than it is today.

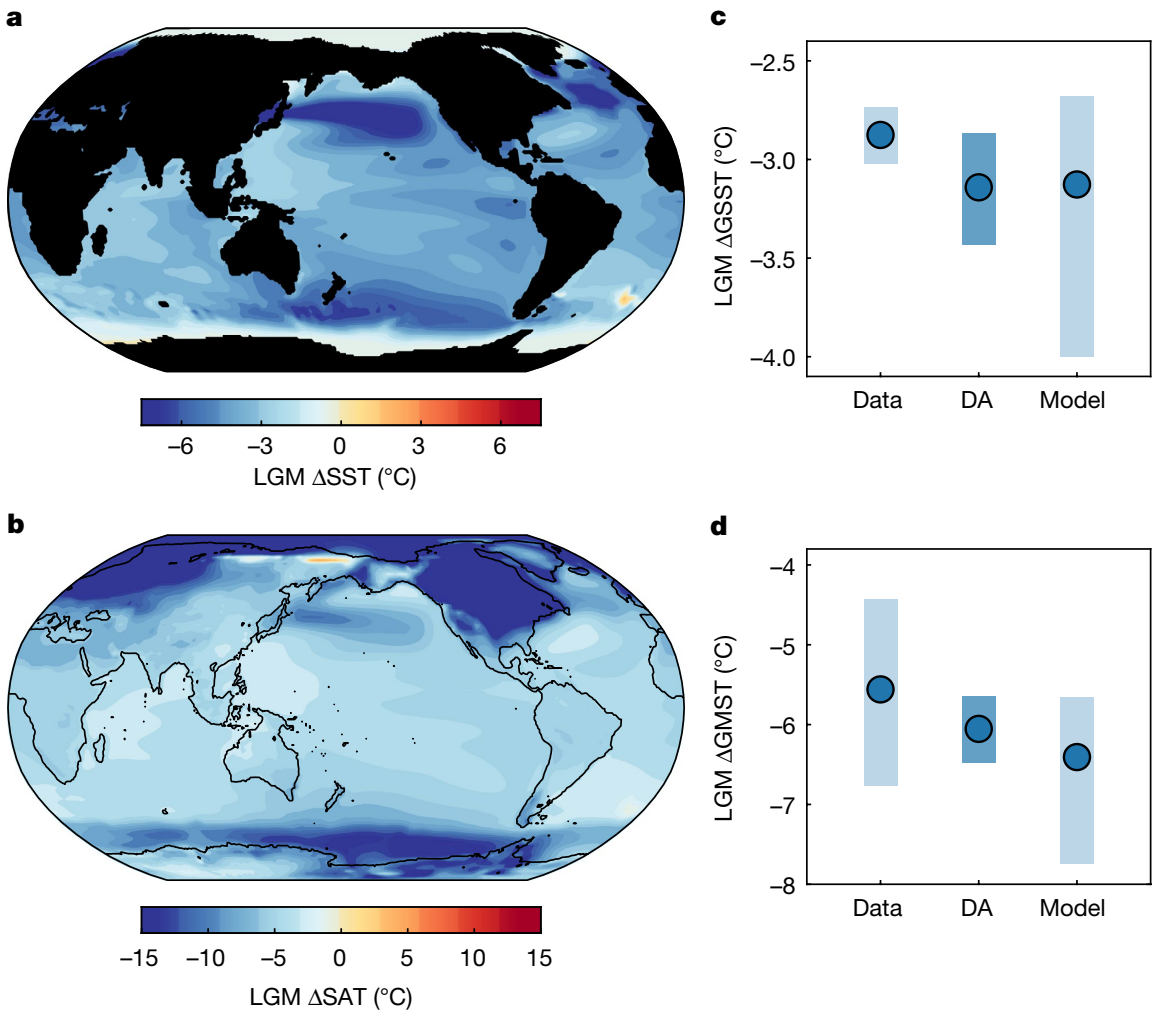

Figure 2.2: Global temperature change (LGM – present). ***a****, The distribution of sea surface temperature change.* ***b****, The distribution of surface air temperature change.* ***c****, Global mean sea surface temperature change.* ***d****, Global mean surface air temperature change. Please note that the circles and bars in* ***c*** *and* ***d*** *represent the median values and 95% confidence interval, respectively. Additionally, the results obtained from data assimilation (DA) are compared with those from prior data and models. Figure from Tierney et al. (2020).*

2.3.2 Geological records

Geological records, including ice cores, sedimentary deposits, and geomorphological evidence, are essential for reconstructing the past glacial environment of the LGM. These geological archives harbor a variety of proxies for past climate patterns and glacial dynamics.

Ice cores

Ice serves as a crucial archive, preserving a wealth of information about the past. Ice cores, drilled from continent-sized ice sheets like Antarctica and Greenland, provide valuable records of past ice and climate conditions, spanning hundreds of millennia (Ruddiman, 2001). Typical

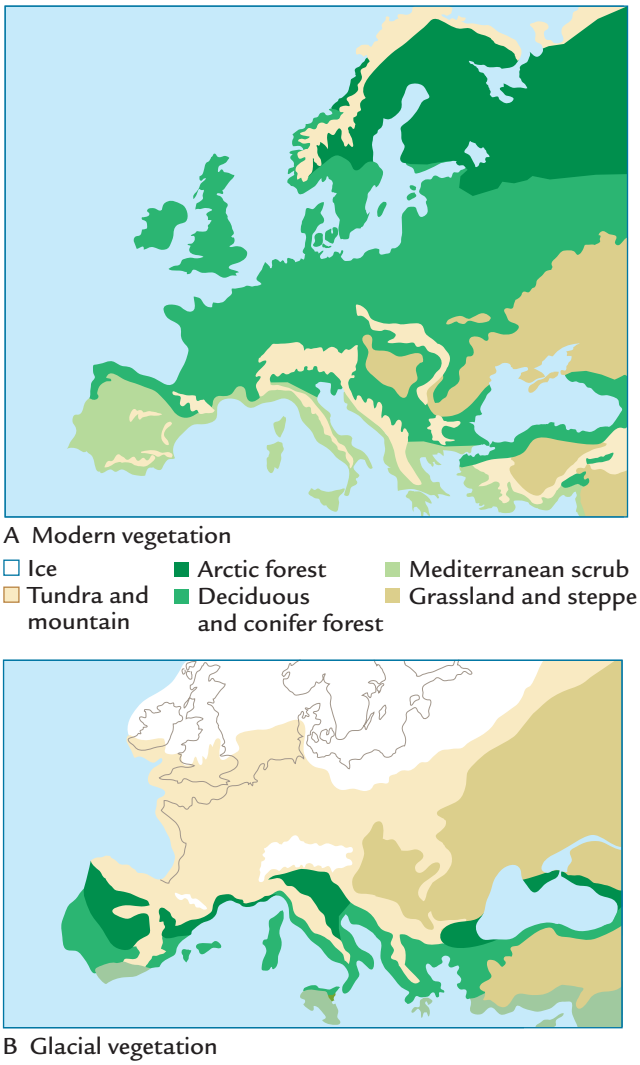

Figure 2.3: The comparison of modern vegetation with that of the LGM, providing insights into the variations in precipitation patterns between the two periods. Figure adapted from Flint (1971).

Analyses of ice cores involve determining the age of the ice layers, studying isotopic composition, and examining the trapped air bubbles. Additionally, radar technology is often utilized to reconstruct the spatial distribution of ice sheets using isochrones.

Isotopic composition, particularly δ^{18}O, serves as a prevalent tool for estimating past temperatures and accumulation rates (Johnsen et al., 1995). An empirical equation has been developed to convert δ^{18}O values into surface temperatures (T, in degrees Celsius) (Johnsen et al., 1989):

$$\delta^{18}O = 0.67 \times T - 13.7‰ \tag{2.9}$$

Figure 2.5 suggests a potential correlation between temperature and δ^{18}O in Greenland, although uncertainties remain regarding the linearity of this relationship.

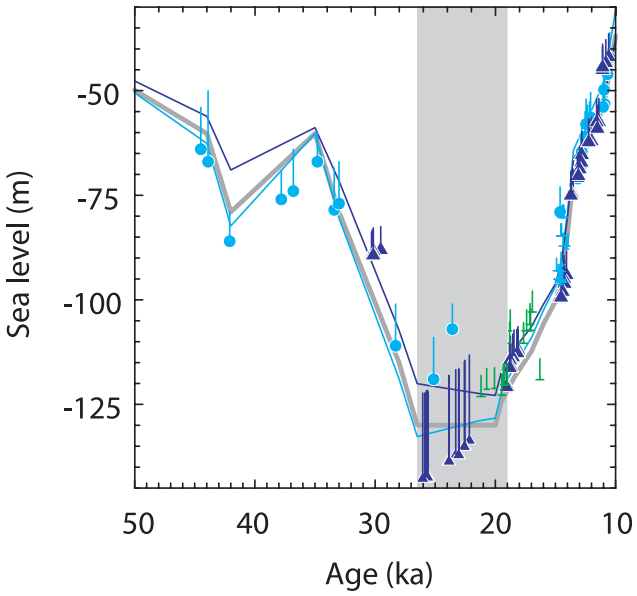

Figure 2.4: Sea-level reconstruction during the LGM. The vertical gray bar denotes the timeframe of the LGM. Figure from Clark et al. (2009).

Sediments

Sediments are essential repositories of geological and biological evidence for reconstructing LGM. Sedimentary records encompass a wealth of information, including shifts in properties like grain size or composition that provide clues about climate and ice sheet dynamics. Moreover, the presence of fossils and annual bands within sediments yields valuable data on past climate conditions, including temperature and precipitation patterns.

Similar to ice core, marine δ^{18}O values from microfossils, such as foraminifera and diatoms, can be used to reconstruct past sea temperatures and ocean conditions. Roughly, a decrease of 1 ‰ in the δ^{18}O ratio corresponds to an increase of 4.2 °C in sea temperature (Ruddiman, 2001). Planktic foraminifera are indicative of sea surface temperatures, while benthic foraminifera reflect deep ocean temperatures.

Geomorphological evidence

The constrains on ice sheets are essential for establishing the boundary conditions for numerical modelling and serve as the foundation for analyzing the complex interactions between climate and ice dynamics.

Reconstructing past ice sheets typically relies on geological mapping of glacial landforms, such as moraines, eskers, and drumlins. The utilization of modern technology, including satel-

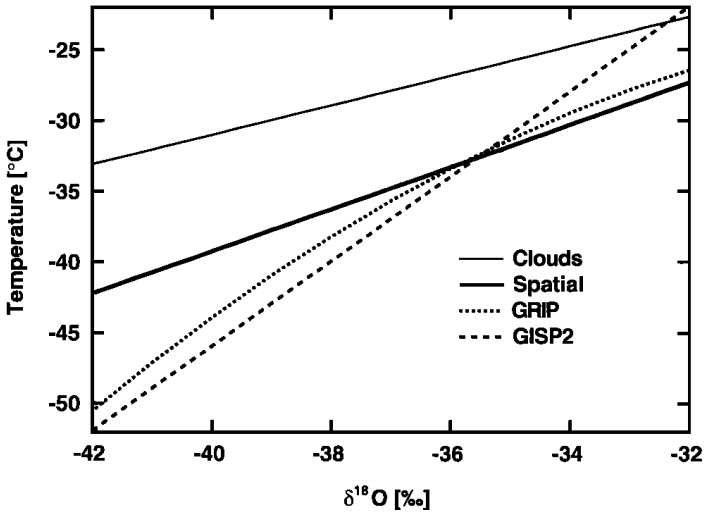

Figure 2.5: The correlation between $\delta^{18}O$ and various types of temperatures in Greenland. The thin line represents the cloud condensation temperature, while the thick line indicates the surface temperature. The dotted curve and the dashed line show the calibration temperature derived from deep boreholes from the Greenland Ice Core Project (GRIP) and the Greenland Ice Sheet Project 2 (GISP2), respectively. Figure from Johnsen et al. (1997).

lite imagery, remote sensing and seismic bathymetry data, greatly aids in the identification and mapping of these glacial features and landforms.

A recent chronological reconstruction of the Eurasian ice sheets during the last glacial cycle was achieved using a newly compiled database (DATED-1) (Hughes et al., 2016). This database is primarily sourced from geomorphological evidence and reliable dating.

Dating methods

Nearly all radiometric dating methods can be applied to date geological records from the LGM. Accurate dating is essential for a trustworthy reconstruction of LGM because it establishes the chronological order of events and their timing.

Radiocarbon dating (^{14}C dating) is a versatile method suitable for dating any carbon-bearing archives, especially valuable for dating deep ocean sediment cores. When properly calibrated, radiocarbon dating yields highly accurate results. Luminescence dating and cosmogenic nuclides dating are commonly employed for dating terrestrial sediments. These two methods exhibit enhanced effectiveness when used in combination, enabling the acquisition of both exposure and burial histories of landforms. Uranium-series dating is notably advantageous in certain field of secondary carbonates, such as reef building corals and speleothems (Scholz and Hoffmann, 2008).

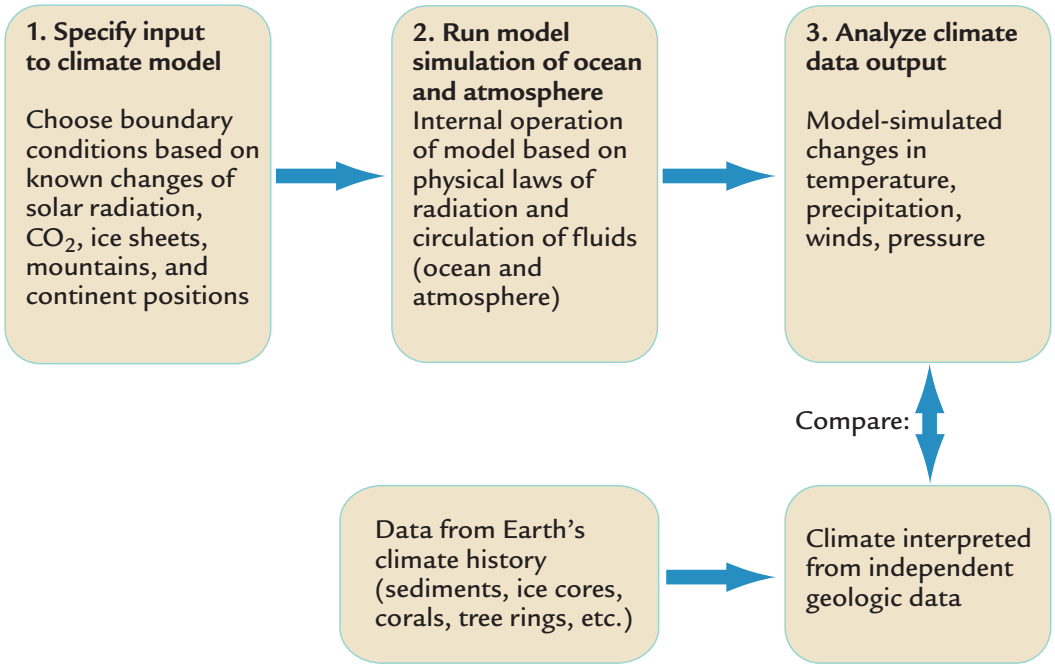

Figure 2.6: The comparison process between simulations and observational data. Figure from Ruddiman (2001).

2.3.3 Numerical modelling

LGM is an ideal period for conducting numerical modelling due to the well-established knowledge of primary boundary conditions, including geography, orbital configuration, and atmospheric CO_2. By utilizing reconstructions derived from geological records, numerical modelling provides a further understanding of past climate and ice sheet dynamics, bridging gaps in observational data. Figure 2.6 illustrates the standard procedures for comparing data with model outputs. Any discrepancies between the two sets may signal various potential issues, such as inaccuracies in model setup or misinterpretations of geological data (Ruddiman, 2001). These mismatches serve as valuable cues for refining boundary conditions, model constructions and data interpretation, ultimately advancing our ability for reconstructing the past.

Numerical modelling stands as a valuable tool for interpreting intricate processes, such as the complex dynamics of large-scale ocean and atmosphere circulation (Li and Battisti, 2008). Furthermore, it offers improved temporal and spatial resolution, a critical component for investigating past glacial-interglacial cycles. Moreover, models serve as a crucial platform for assessing hypotheses put forward by paleoclimatologists and glaciologists. By examining diverse scenarios, researchers can quantify the influence of various parameters to climate change.

The reconstruction of LGM benefits from a collaborative approach that combines observational data interpretation and numerical modelling. Reconstructing past conditions advances most when both data and models are constantly tested against each other, acknowledging their respective strengths and limitations.

2.4 Potential key mechanisms for glacial inception and termination

Ice sheets undergo periodic advances and retreats, giving rise to glacial-interglacial cycles. Extensive research using proxy records has revealed that ice sheets exhibit a sawtooth shape, characterized by slowly growth and rapid termination, over geological time scales (Abe-Ouchi et al., 2013). However, the precise mechanisms governing glacial inceptions and terminations remain largely elusive. This complexity largely stems from the nonlinear responses of ice sheet to climate variations (Paillard, 1998). Nevertheless, there is a broad consensus that factors linked to temperatures and moisture contents play pivotal roles in initiating and terminating glacial phases (Haug et al., 2005).

2.4.1 Temperature-related mechanisms

Energy balance is a critical factor that decisively shapes Earth's surface temperature, which, in turn, plays a vital role in both climate and cryosphere systems. Numerous studies have highlighted a robust connection between insolation (incoming solar radiation) and ice volume (e.g., Hays et al., 1976; Huybers, 2011; Lisiecki, 2010). This relationship becomes particularly pronounced when dealing with large ice sheets, as even a modest increase in insolation can trigger a fast termination (Abe-Ouchi et al., 2013). Additionally, internal feedback mechanisms, such as albedo feedback and atmospheric CO_2 variations, can significantly influence the amount of energy absorbed by Earth, consequently leading to shifts in temperature and ice volume.

Insolation

Among the various potential mechanisms, Milankovitch's orbital theory remains the predominant explanation for the onset and termination of glaciations (Hays et al., 1976; Lunt et al., 2008). The glacial-interglacial cycles exhibit significant alignment with Earth's key orbital pa-

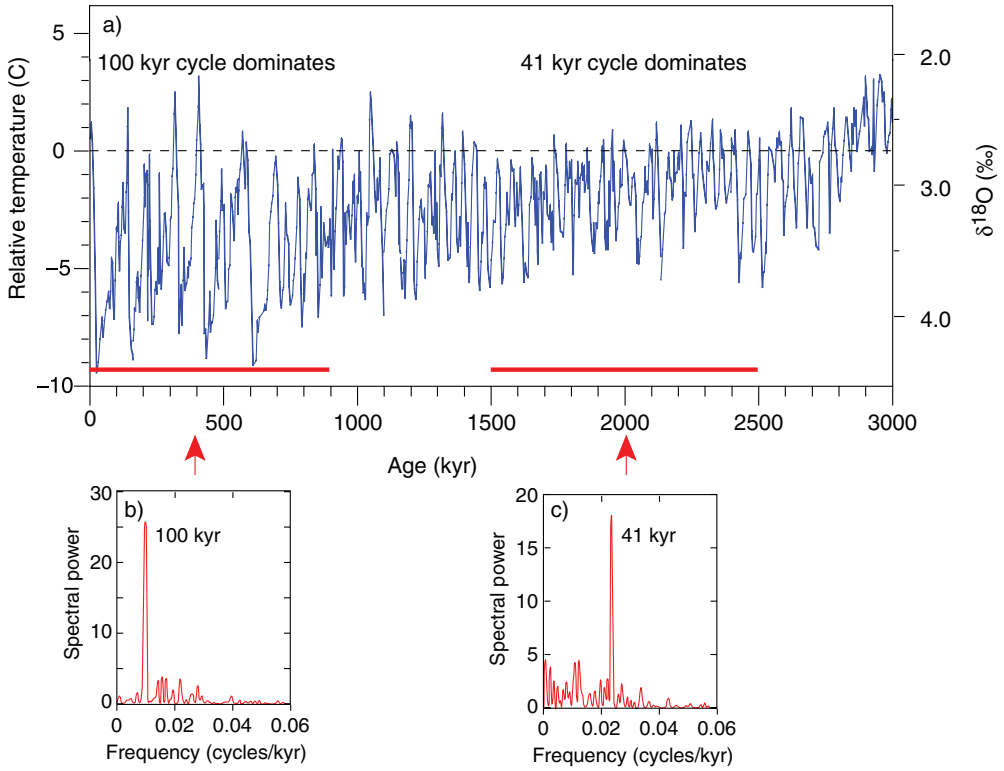

Figure 2.7: Glacial cycles over the past 3 million years, reconstructed using a benthic $\delta^{18}O$ record from the North Atlantic. It is worth noting that for the past million years, it is dominated by 100-kyr cycle. However, for the earlier part, the 41-kyr cycle held greater prominence. Figure from Kirkby and Carslaw (2006).

rameters: precession (23 kyr), obliquity (41 kyr) and eccentricity (100 kyr), as evident from paleoclimate records (Hays et al., 1976; Huybers, 2011; Lisiecki, 2010). While the 23-kyr and 41-kyr glacial-interglacial cycles can be largely explained by insolation variations linearly (Imbrie et al., 1992), the 100-kyr problem remains elusive due to the absence of clear explanations for forcing this periodicity (Figure 2.7). Notably, there are limited changes in insolation forcing in this frequency band (Paillard, 1998).

One proposed solution to this challenge involves the concept of multiple equilibria within the climate system, where nonlinear mechanisms may contribute to understanding this periodicity (Paillard, 1998). In his work, Paillard (1998) employed a conceptual model featuring three distinct states of ice volume. Remarkably, this model successfully replicated every glacial-interglacial cycle with accurate timing and amplitude over the late Pleistocene, including the onset of 100-kyr glacial cycles. However, the precise identification of critical thresholds for different states is still a subject of ongoing research. An alternative perspective suggests that the 100-kyr problem may solely result from internally processes related to the interaction of isostatic adjustment and the elevation-mass balance feedback (Oerlemans, 1980).

Abe-Ouchi et al. (2013) propose that the 100-kyr periodicity is explained by a combination of insolation changes and internal feedbacks, including delayed bedrock rebound, ice-sheet margin calving, CO_2 variations, ocean feedback and dust feedback.

Nonetheless, the initiation of Last Glacial Period and the onset of Northern Hemisphere glaciation are both proposed to be linked to the point when summer insolation reached its minimum (Haug et al., 2005; Risebrobakken et al., 2007). Some theories even suggest that a potential alternation in total solar radiation during these periods, although this hypothesis remains untestable due to the lack of relevant data (Öpik, 1958).

Albedo-temperature feedback

Snow or ice has significantly lower albedo compared to land or water surfaces. As ice sheets expand or shrink, they can either reflect or absorb more solar radiation, leading to further cooling or warming effects. This positive feedback mechanism is estimated to amplify the initial climate change by about 40% (Ruddiman, 2001). For instance, a 1 °C cooling would be amplified to 1.4 °C cooling due to this albedo-temperature feedback.

Furthermore, it is suggested that the cold climate during LGM is largely attributed to the extensive size of ice sheets, which reflected a substantial amount of solar radiation, despite summer and winter insolation being similar to present-day conditions (Ruddiman, 2001).

Greenhouse effect

As one of the primary greenhouse gasses, atmospheric CO_2 has long been considered closely linked to glaciation and deglaciation. It is postulated that reduced atmospheric CO_2 levels can result in diminished heat trapping, leading to lower temperatures and reduced ablation due to a weakened greenhouse effect. When atmospheric CO_2 falls below a certain threshold, it may significantly contribute to the initiation of a glaciation. Notably, recent research suggests that the Greenland glaciation during Late Pliocene was controlled by declining atmospheric CO_2 levels, although the precise reasons for this decline remain a subject of ongoing investigation due to the scarcity of direct pre-Quaternary indicators (Lunt et al., 2008). Nevertheless, CO_2 reacts rather slowly to changes in ice volume, making it less influential during the initial phases of glacier growth and decay.

2.4.2 Moisture-related mechanisms

Unlike the relatively well-established mechanisms associated with temperature, those connected to moisture supply in the initiation and termination of glaciation remain largely uncertain (Haug et al., 2005).

The Atlantic Meridional Overturning Circulation (AMOC) represents another key factor influencing glaciation and deglaciation processes. AMOC plays a critical role in heat redistribution, which directly affects sea surface temperature, influencing evaporation, thus moisture availability, and precipitation patterns. This, in turn, can potentially contribute to both the onset of glaciations and the acceleration of deglaciation. The influx of freshwater from melting ice sheets can alter ocean salinity, leading to a reduction in AMOC strength. While one perspective suggests that the onset of glaciation coincides with a weakened AMOC that transports less heat to high latitudes (Cortijo et al., 1994), Risebrobakken et al. (2007) suggest an opposing viewpoint. They argue that AMOC was enhanced at the initiation of Last Glacial Period, resulting in increased storminess and moisture transport, thereby promoting greater winter precipitation that facilitated ice sheet growth (Risebrobakken et al., 2007).

Haug et al. (2005) propose an alternative hypothesis, suggesting that North Pacific seasonality leads to changes in water vapor supply, which in turn encourages the initiation of Northern Hemisphere glaciation. Their research indicates that, despite annually cooling, late summer warming extending into autumn sustains moisture supply to North America, while cold spring conditions reduce snow melt (Haug et al., 2005).

Tectonic processes also have the potential to alter precipitation pattern. One hypothesis suggests that the tectonically driven closure of the Panama seaway led to an increased northward flow of atmospheric moisture, resulting in greater snowfall. This hypothesis finds support in coincidental changes in salinity and Ice Rafted Debris (IRD) at the same timing (Haug and Tiedemann, 1998; Keigwin, 1982). Another proposal is that the uplift of the highlands, such as the Rocky Mountains and Himalayas, could introduce cooler air and additional moisture, leading to increased snowfall and the initiation of Northern Hemisphere glaciation (Ruddiman and Kutzbach, 1989). However, it is worth noting that some researchers argue that these tectonic mechanisms may not be substantial enough to significantly contribute to Northern Hemisphere glaciation (Lunt et al., 2008). For LGM, tectonic mechanisms are likely to have played a minor role, given that its tectonic setting closely resembled the present-day conditions.

Changes in storm trends can significantly impact precipitation levels. When storm tracks shift, it can result in inverse changes in annual precipitation between two regions (Rasmussen and Conway, 2004). Furthermore, elevation desertification is particularly evident in high and cold regions, causing a self-limiting tendency for ice sheets. As an ice sheet grows, it tends to experience reduced moisture content, which constrains its further growth (Cuffey and Paterson, 2010).

2.4.3 Other potential mechanisms

In addition to the mechanisms mentioned above, several other potential mechanisms may also contribute to the initiation and termination of glaciation.

One perspective suggests the volcanic activity may contribute to trigger glaciation, given that significant aerosols and gases released by volcanic eruptions can result in sunlight blocking and cooling effects. Evidence indicates that there might be a higher rate of explosive volcanism during the Quaternary (Kennett and Thunell, 1975). This mechanism has been demonstrated to potentially explain some instances of glaciation initiation (Maslin et al., 1998). However, it is worth noting that while volcanic eruptions can initially induce cooling, they may contribute to long-term warming through greenhouse effect, potentially aiding deglaciation.

Delayed rebounding of Earth's crust is suggested to have made a significant contribution to the fast termination of ice sheets by maintaining the surface elevation at relatively low levels (Deblonde et al., 1992; Oerlemans, 1980; Pollard, 1982).

Additionally, some more alternative factors are proposed for contributing the initiation of glaciation. For example, it has been proposed that the termination of a permanent El Niño-like state in Late Pliocene may have triggered the inception of Northern Hemisphere glaciation (Wara et al., 2005). However, it is worth noting that this hypothesis has been challenged by Lunt et al. (2008). Recent advances in the field have provided new insights. For instance, gradual cooling in the tropical Pacific is suggested to have played a role initiating glaciation in North America, although the exact cause of this cooling in the tropical Pacific remains a puzzle (Huybers and Molnar, 2007). Moreover, the increased glaciation of Antarctica may have contributed to the intensification of Northern Hemisphere glaciation by fundamentally altering deep ocean circulation patterns that lead to heat redistribution (Woodard et al., 2014).

2.4.4 Summary

It's crucial to note that ice-climate system is highly complex. The initiation and termination of glaciation are rarely attributable to one single mechanism. Instead, multiple feedback mechanisms interact collaboratively, giving rise to tipping points where even minor changes can trigger significant and irreversible shifts in ice sheet growth or collapse.

While the analysis of reconstructed data frequently encounters practical limitations, numerical modeling provides a window into the complexity of interactions by probing different processes individually. It aids in gaining essential insights into the intricate interactions crucial for understanding past glaciations and deglaciations, as well as for making predictions about future climate changes.

Chapter 3

Data and methods

3.1 BESSI

3.1.1 Model setup

The surface energy and mass balance model, BESSI, is applied to calculate the spatial and temporal variations of SMB. In this study, the domain encompasses the entire Northern Hemisphere, centered on the North Pole (313×313 grid cells, with the resolution of 40 km). The vertical dimension comprises approximately 15m with a maximum of 15 layers, covering the maximum depth of seasonal temperature variability (Born et al., 2019). Each column on the horizontal grid can have a varying number of vertical layers. Within each column, processes such as melting and refreezing can occur, leading to fluctuations in the snow mass. If a single layer exceeds the maximum threshold of 500 kg/m^2, it splits into two, with 300 kg/m^2 remining in the original layer, and 200 kg/m^2 transferring to the layer below. This continues until there are 15 layers, at which point any excess snow mass is removed from the column. The minimum threshold is set at 100 kg/m^2, and if a layer contains less than this threshold, it merges with the layer below (Born et al., 2019). Temperature and density remain constant, while the distribution of liquid water follows the same ratio as that used for snow after the split (Figure 3.1). For more detailed introduction of BESSI regarding the physical processes, please refer to Born et al. (2019) and Zolles and Born (2021).

The parameters utilized by BESSI are calibrated to the Regional Atmospheric Climate Model (RACMO), which provides a valuable resource for addressing climate-related challenges at the regional level (Noël et al., 2016). Additionally, they are fined-tuned using data

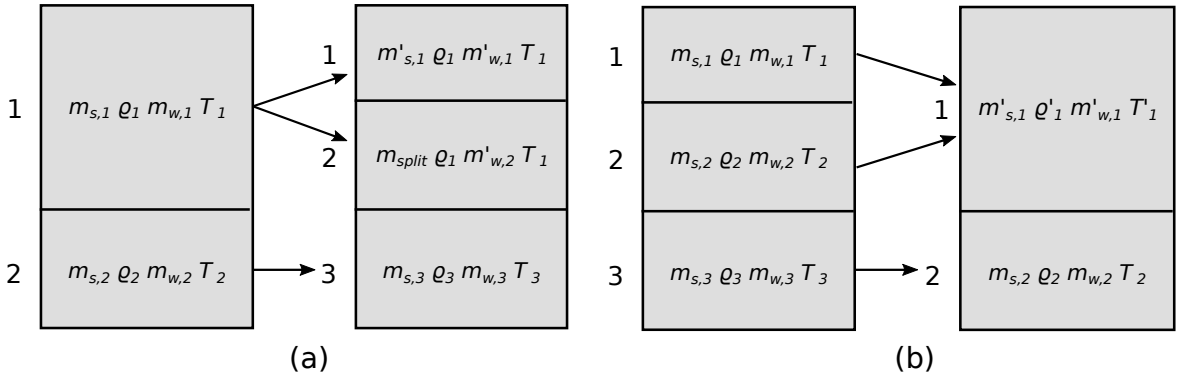

Figure 3.1: (a)Splitting one layer into two layers if it exceeds 500 kg/m^2. (b) Merging two layers if the upper layer drops below 100 kg/m^2. Figure from Born et al. (2019) .

from GRACE satellite (Zolles and Born, 2022).

3.1.2 Numerical implementation

BESSI iterates with a daily time step. Figure 3.2 shows the decision tree for each grid cell at each step. Densification, diffusion, percolation and the surface energy balance are calculated at each time step to account for all relevant physical mechanisms, grounded in fundamental physical principles, while maintaining computational efficiency. In particular, BESSI rigorously adheres to the principles of energy and mass conservation.

In this study, we utilize a back-and-forth climate looping approach, rather than a one-way repeating of forward or backward order. The intention behind this choice is to mitigate abrupt changes that may not align with realistic conditions, thereby minimizing the potential for unrealistic SMB calculations. Each SMB simulation runs for 500 years, considering the extended response time required for the firn cover to attain both dynamical and thermodynamical stability (Zolles and Born, 2021). The necessity for a stable firn cover arises from its role as the foundation for accurately calculating SMB, ensuring a reliable reflection of accumulation and ablation processes. The results from the final year (i.e., the 500^{th} year of the simulation) are interpreted.

3.2 Input data

BESSI requires five essential climate fields obtained from climate forcing data: surface air temperature, total precipitation, shortwave radiation, longwave radiation, and humidity. The climate reference height is also sourced from climate forcing data. These variables are all in-

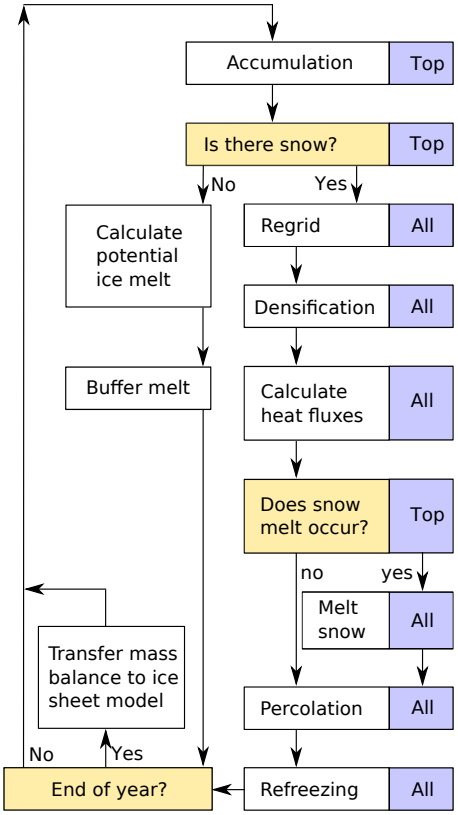

Figure 3.2: Flowchart for each time step, where the crucial questions in the logic tree are indicated by the yellow boxes. The blue boxes specify whether the top layer or all layers are taken into account. Figure from Born et al. (2019) .

terpolated bilinearly onto the BESSI grid. For current topographic information, the ETOPO5, a high-resolution digital elevation model (DEM) dataset is utilized.

3.2.1 Climate forcing

In this study, we employ a classical snapshot method to obtain climate forcing data. The current climate forcing data are sourced from the ERA5 reanalysis dataset, while data for the LGM climate forcing are derived from the Community Climate System Model, version 4 (CCSM4). To estimate climate forcing for intermediate periods, we utilize these two snapshots in combination with a weighting factor (η). This factor acts as a glacial index, indicating the degree to which the climate resembles LGM conditions.

This study employs daily transient climate forcing, which is considered to be the optimal choice for the surface mass balance model (Zolles and Born, 2022).

The ERA5 reanalysis

ERA5, produced by the European Centre for Medium-Range Weather Forecasts (ECMWF), is one of the most advanced global reanalysis datasets. It is widely used for studying climate dynamics (Hoffmann et al., 2019).

To successfully incorporate climate data into BESSI, a series of unit conversions are conducted to ensure that the variables are in strict adherence to BESSI's analysis requirements. Subsequently, all the variables are interpolated bilinearly onto the BESSI gird. Following this interpolation, a few points exhibited slightly negative precipitation values (less than -10^{-8} mm/day), which are all set to zero.

LGM forcing from CCSM4

The Community Climate System Model, version 4 (CCSM4), serves as a comprehensive tool for studying Earth's climate system interactions and for understanding past, present, and future climate patterns and variability. Although uncertainties persist in the LGM forcing, it has been demonstrated that the simulated LGM sea ice coverage aligns well with the global proxy reconstructions and syntheses (Brady et al., 2013).

This study primarily focuses on temperature and precipitation fields in the LGM forcing to produce climate anomalies distinct from current conditions. Similar to the procedure employed for the ERA5 dataset, unit conversion is executed to meet the requirements of BESSI. Subsequently, the LGM forcing is bilinearly interpolated onto the grid of BESSI.

Climate anomalies

Minimizing uncertainties stemming from different climate models is crucial to generating more accurate climate anomalies between LGM and current climate conditions. Consequently, the historical dataset derived from second version of the Community Earth System Model (CESM2) is utilized to represent the current climate conditions. Given that CESM2 builds on the foundations of CCSM4 and they are both developed by the National Center for Atmospheric Research (NCAR), the uncertainties associated with using distinct climate models are largely mitigated.

In this study, both temperature and precipitation anomalies are derived from the historical dataset from CESM2 and the LGM dataset from CCSM4.

1) Temperature anomalies

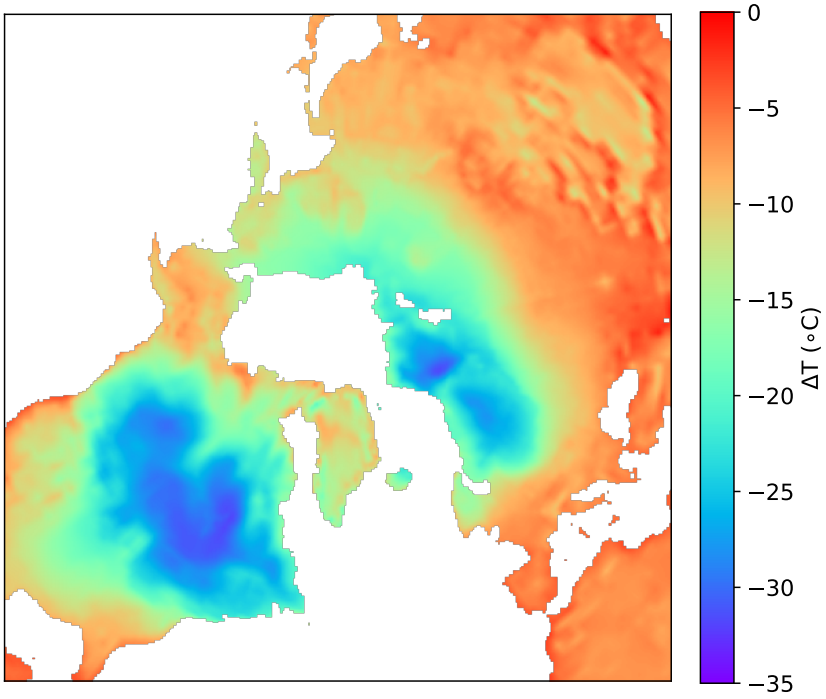

Figure 3.3: Annual mean temperature anomaly ($T_{LGM} - T_{PD}$).

A daily climatology, representing a typical LGM year, was calculated using the 30-year LGM dataset derived from CCSM4. In parallel, a daily climatology for the reference period 1980-2009 was obtained from the historical dataset to represent a typical present-day year. The temperature anomaly (ΔT) between LGM and current period is then established by subtracting the typical present-day year from the typical LGM year. Figure 3.3 illustrates the distribution of the annual mean temperature anomaly between LGM and present time. Notably, all regions show a temperature decrease for the LGM period, with areas covered by the ice sheet displaying the most pronounced temperature drop (Figure 3.1).

Subsequently, different temperature anomalies are generated using certain amount of ΔT:

$$T = T_{ERA5} + \eta \times \Delta T \tag{3.1}$$

where T represents the temperature after incorporating temperature anomalies. T_{ERA5} is the current temperature from the ERA5 reanalysis. η serves as a weighting factor; smaller η values make the temperature (T) approach the current temperature (T_{ERA5}), while larger η values make the temperature (T) resemble the LGM temperature.

2) Precipitation anomalies

The precipitation variable is also a three-dimensional parameter in both datasets. The pro-

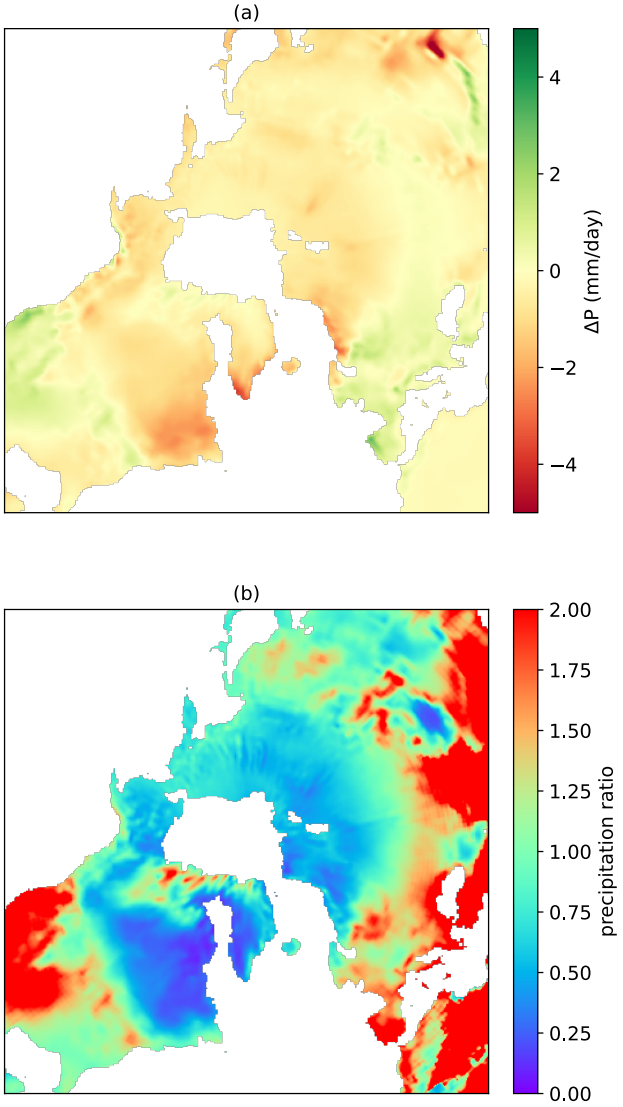

Figure 3.4: ***(a)*** *Annual mean precipitation anomaly ($P_{LGM} - P_{PD}$).* ***(b)*** *Annual mean precipitation ratio* $\left(\frac{P_{LGM}}{P_{PD}}\right)$. *Note that virtually all areas covered by ice during LGM have a precipitation ration below 2.*

cess mirrored that of temperature, with the typical LGM year and the typical present-day year calculated identically the same. The precipitation anomaly (ΔP) is determined by subtracting the current precipitation from the LGM precipitation. Figure 3.4 presents the distribution of the annual mean precipitation anomaly between LGM and current conditions. Interestingly, unlike the temperature anomaly, precipitation displays bidirectional variations. Regions that were once covered by ice sheets in North America and Eurasia experienced aridity during LGM, while the Mediterranean and the southern parts of North America were wetter during the same period (Figure 3.4**a**).

Using the same anomaly approach as for temperature would lead to negative precipitation values. Therefore, we use relative anomalies instead (Figure 3.4**b**). The ratio is calculated by

dividing the LGM precipitation by current precipitation. The limitation of below 2 is due to the majority of investigated areas exhibiting rations below this threshold.

Subsequently, precipitation anomalies were generated using precipitation ratio:

$$P = P_{ERA5} \times \left(\frac{P_{LGM}}{P_{PD}} \right)^{\eta} \tag{3.2}$$

where P represents precipitation after integrating precipitation anomalies. P_{ERA5} is the current precipitation from the ERA5 reanalysis. $\frac{P_{LGM}}{P_{PD}}$ denotes the precipitation ratio. η serves a weighting factor; smaller η values cause precipitation (P) to approach the current precipitation (P_{ERA5}), while larger η values make precipitation (P) resemble LGM precipitation.

3.2.2 Topography and climate reference height

Topography anomalies

In this study, we use ETOPO5 as the present-day topographic dataset. ETOPO5 is a global relief model characterized by a horizontal resolution of 5 arc minutes. Due to this high resolution, it is widely used in research. The ice sheet thickness during LGM is obtained from Paleoclimate Modeling Intercomparison Project Phase 3 (PMIP3) in conjunction with the Couped Model Intercomparison Project Phase 5 (CMIP5). The LGM PMIP3-CMIP5 experiment employed a composite ice sheet reconstruction compiled from three data sources, enhancing the comparability across different models (Abe-Ouchi et al., 2015). While there may be room for improvements, it is improbable that the ice sheet configuration deviated significantly from the actual conditions during the LGM (Abe-Ouchi et al., 2015). Figure 3.5 illustrates the present-day topography and ice thickness relative to the present. The topography anomalies are created using a specific value of the additional LGM ice thickness (h):

$$Z = ETOPO5 + \eta \times h \tag{3.3}$$

where Z signifies the topography after incorporating some topography anomalies. $ETOPO5$ represents topographic information from ETOPO5. η serves a weighting factor, smaller η values make topography (Z) approach the current topography ($ETOPO5$), while larger η values make topography (Z) resemble LGM topography. If η>1, topography (Z) exceeds LGM topography.

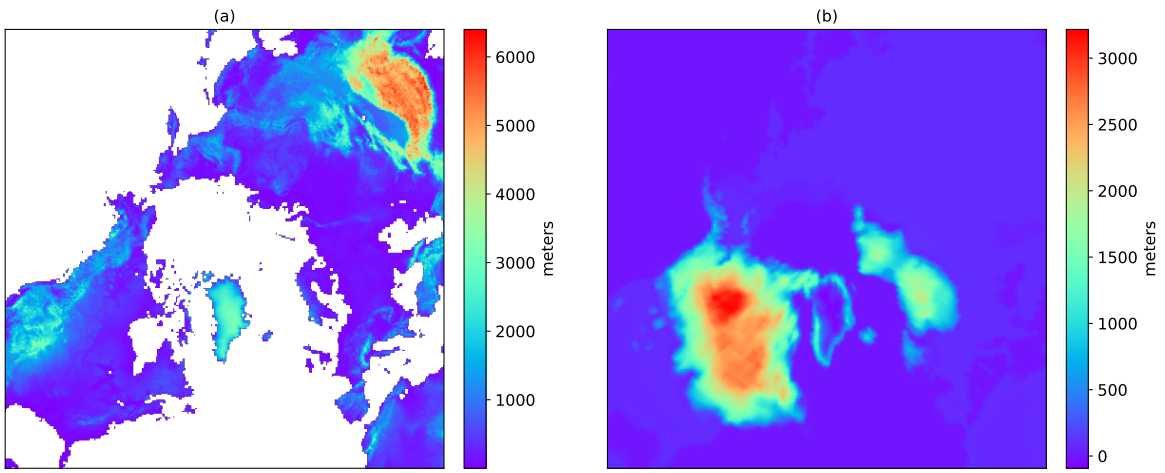

Figure 3.5: ***(a)*** *Current topography derived from ETOPO5.* ***(b)*** *Additional ice thickness in comparison to the present conditions, obtained from PMIP3-CMIP5. Note that large areas in North America and Eurasia were covered with ice during LGM.*

Climate reference height anomalies

In this study, the LGM climate reference height is derived from the LGM dataset from CCSM4, while the current climate reference height is obtained from the ERA-interim reanalysis. Given that the ERA-interim reanalysis dataset is produced by the same company as ERA5 reanalysis dataset, any differences are likely negligible. By subtracting the current climate reference height from the LGM climate reference height, the climate reference height anomaly between LGM and present time (CR_{LGM}) is obtained. Subsequently, by introducing a specific value of CR_{LGM}, a new climate reference height (CR) with anomalies is created:

$$CR = CR_0 + \eta \times CR_{LGM} \tag{3.4}$$

where CR signifies the climate reference height after incorporating anomalies. CR_0 is the climate reference height from ERA-interim dataset. η serves a weighting factor; smaller η values make the climate reference (CR) approach the current one (CR_0), while larger η values make the climate reference (CR) resemble the LGM climate reference.

3.3 Surface Mass Balance (SMB) simulations

In this study, we conduct simulations of several SMB series to investigate the intrinsic relationship between SMB and key variables, such as temperature, precipitation and topography. We use the scaling factor η to gain insights into the evolution of SMB along the glaciation

process (or deglaciation process when analyzing the results in reverse order). Specifically, we choose 10 different values for η, ranging from 0.2 to 2 in increments of 0.2. It is worth noting that when $\eta = 1$, it corresponds to full glacial (LGM) conditions, while $\eta > 1$ signifies an even more severe glaciation than LGM.

We primarily investigate three variables: Temperature (T), Precipitation (P), and Topography (Z), in combination with modifications to other corresponding variables such as climate reference height (CR) and sea-level offset (SL offset). Table 3.1 provides the detailed information on how these different series of simulations are constructed. For instance, in the first series of simulation (Varying_T), we utilize varying temperature calculated from equation 3.1, while keeping precipitation, topography, and climate reference height fixed at LGM values (Table 3.1). Given that the sea level was about 125 meters lower than present during LGM, we set the sea level offset to be -125 m.

Table 3.1: Different series of SMB simulations.

Series	T	P	Z	CR	SL offset (m)
Varying_T	**Eq.** (3.1)	P_{LGM}	Z_{LGM}	CR_{LGM}	-125
Varying_P	T_{LGM}	**Eq.** (3.2)	Z_{LGM}	CR_{LGM}	-125
Varying_Z	T_{LGM}	P_{LGM}	**Eq.** (3.3)	CR_{LGM}	$\eta \times (-125)$
Varying_TP	**Eq.** (3.1)	**Eq.** (3.2)	Z_{LGM}	CR_{LGM}	-125
Varying_all	**Eq.** (3.1)	**Eq.** (3.2)	**Eq.** (3.3)	**Eq.** (3.4)	$\eta \times (-125)$

In additional to conducting a comprehensive analysis of SMB evolution in response to changes in key variables, we also zoom in on specific time intervals, including the present day (indicated by η ranging from 0 to 0.2 in increments of 0.02) and the LGM (indicated by η ranging from 0.9 to 1.1 in increments of 0.02). We primarily use two series of simulations, which are Varying_T and Varying_P, to assess the relative significance of temperature and precipitation and to gain insights into which factor plays a dominant role during glacial inception and termination.

Our study encompasses the entire Northern Hemisphere. However, different continental ice sheets exhibited distinct behaviors during the Last Glacial Period. For instance, the North

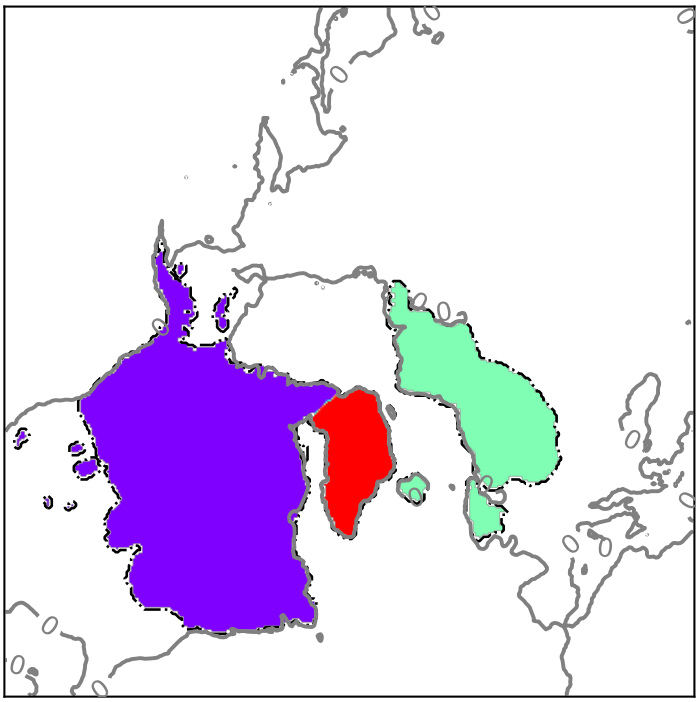

Figure 3.6: Land masks for North America (purple), Eurasia (green) and Greenland (red). The contour represents elevations at 0 meters, derived from the LGM topography, which combines ETOPO5 with the ice thickness relative to present (as indicated by PMIP3-CMIP5).

American ice sheets underwent a dramatical increase from glacial inception to the LGM, while the Eurasian ice sheets experienced relatively minor changes between these two phases (Liakka et al., 2016). To facilitate our analysis, we generate land masks to separately study three crucial regions: North America (NA), Eurasia and Greenland (Figure 3.6). The boundaries of the land masks are determined by the maximum extent of ice sheets during the Last Glacial Period, specifically corresponding to the areas where the ice sheets expanded during the LGM as indicated by PMIP3-CMIP5.

Chapter 4

Results

4.1 Control simulation

A control case is a fundamental component of modeling, as it evaluates the model's performance and accuracy in current scenarios, which in turn ensures its reliability for exploring past and future scenarios. In this study, we use ERA5 as current climate forcing and ETOPO5 as current topography. The model is run for 500 years using the years 1961-1990 as input in a back-and-forth loop to smooth out abrupt changes that may not correspond to realistic conditions. Figure 4.1**a** shows the spatial distribution of SMB in Northern Hemisphere simulated by BESSI. It is noteworthy that most non-dark-blue areas, signifying more positive SMB, correspond to regions covered by glaciers. This observation aligns with previous research findings suggesting that mountain glaciers of larger size tend to exhibit more positive SMB (Schuler et al., 2020). One additional aspect that deserves attention is that these non-dark-blue places (indicating more positive SMB) do not necessarily correspond to high altitudes but could be attributed to high latitudes. Both factors, high altitudes and high latitudes, have played significant roles in causing more positive SMB.

To specifically assess the simulated SMB, we focus on Greenland, one of the most intensively studied regions in the Northern Hemisphere, and compare our result (Figure 4.1**b**) with those of other researchers (Figure 4.2 Fettweis et al., 2020). Please take note that Figure 4.1**b** and Figure 4.2 use two different colormaps. Our findings align closely with previous studies, revealing a consistent pattern of SMB distribution: more positive SMB in the south, especially in the southeastern part of Greenland, while more negative SMB is found along the edges of Greenland. Note also that an earlier version of BESSI was included in Fettweis et al. (2020).

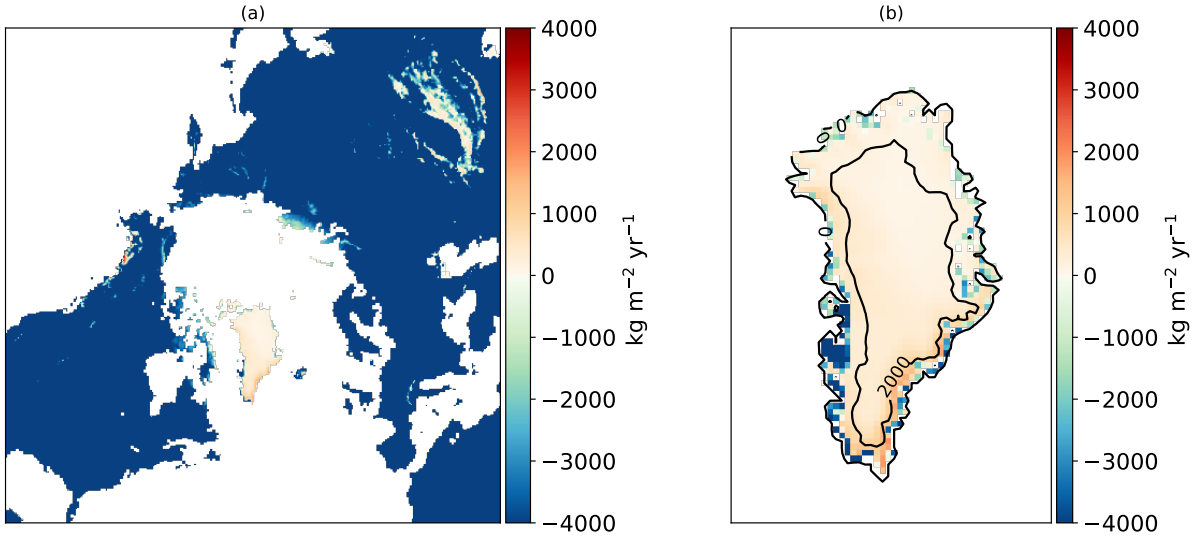

Figure 4.1: Spatial distribution of SMB by BESSI from the control case under current conditions. ***(a)*** *In the Northern Hemisphere.* ***(b)*** *On Greenland. Contours represent elevations of 0 meters and 2000 meters, respectively.*

The adequate accuracy demonstrated by the control case provides a foundation for subsequent analyses.

4.2 SMB sensitivity to increasing glacial severity

By utilizing the key glacial index factor η (ranging from 0.2 to 2 in increments of 0.2) to control the changing variables, we generate five series of mean SMB evolutions corresponding to increasingly severe glacial conditions, as indicated by higher η values. Our primary focus centers on three key regions that were covered by ice sheets during the LGM: North America (NA), Eurasia and Greenland (Figure 3.6). And we conduct individual analyses for each of these regions. While the overall trend is largely consistent, some small discrepancies persist among these three regions.

4.2.1 SMB response to changes in key variables

Temperature and precipitation are two primary factors directly regulating SMB, prompting us to explore how changes in temperature and precipitation impact SMB. In this study, we conduct three series of simulations, denoted as Varying_T, Varying_P and Varying_TP, to examine how SMB responds to changes in temperature, precipitation, and both. Topography is another critical factor influencing SMB. Therefore, we assess the independent impact of to-

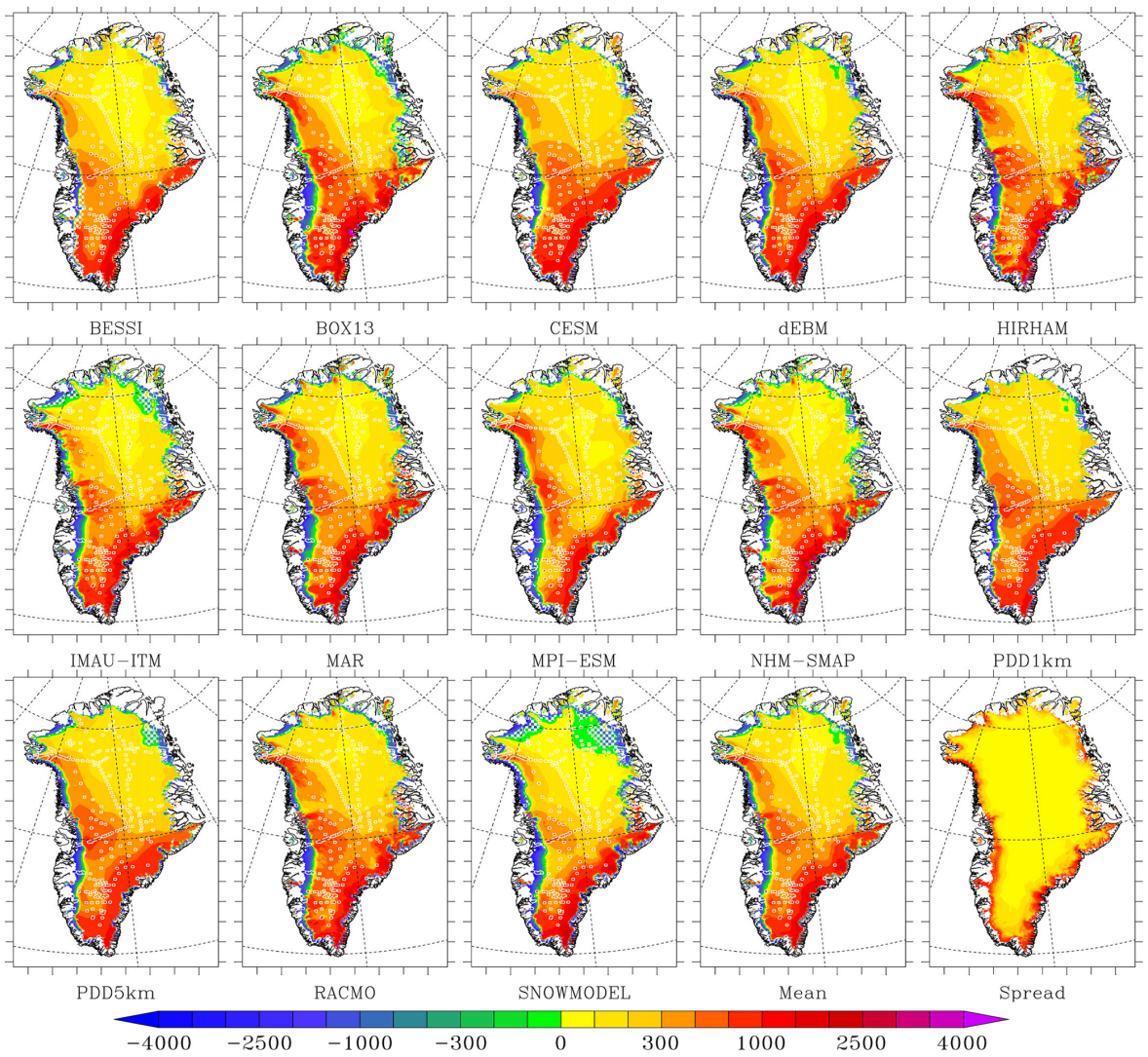

Figure 4.2: Greenland's simulated SMB (kg m^{-2} yr^{-1}) by 13 models, with white circles indicating the field data used for model evaluation. Note that the scale is nonlinear, with a smaller step (100) for absolute SMB values below 500, while a larger step (500) for values exceeding 500. Note that BESSI is one of the model ensembles. Figure from Fettweis et al. (2020).

pography on SMB through the Varying_Z simulations. Furthermore, we examine how SMB reacts to changes in all the key variables (temperature, precipitation, topography) through the of Varying_all simulations.

It is worth emphasizing that all other variables are held constant at LGM values, except for the variable(s) under investigation.

Varying_T

Figure 4.3 illustrates the variation in SMB in response to temperature changes for the three key regions. All three regions exhibit a similar evolution pattern. Initially, a slight increase

in the glacial temperature anomaly leads to a rapid rise in SMB, possibly due to a significant shift from rainfall to snowfall. However, as η increases, this effect diminishes, and the slope gradually levels off. This could be attributed to the fact that as more areas experience freezing conditions, further temperature reductions have limited impact on the conversion of rainfall into snowfall.

While the overall trend closely resembles, it is worth noting that the variations in SMB caused by temperature changes are significantly less pronounced for Greenland compared to NA and Eurasia. This discrepancy may be attributed to the fact that the majority of Greenland is already sufficiently cold even at present-day climate, and further reduction in temperature does not cause dramatic positive effects on SMB. Moreover, NA experiences a more rapid growth compared to Eurasia.

It is important to elucidate why the mean SMB for Greenland at $\eta = 0$ is clearly negative. This can be attributed to two factors. First, the land mask we use to represent the Greenland ice sheet during the LGM encompasses a larger area than present-day Greenland, potentially incorporating more regions with negative SMB outside the current boundaries. Second, we use the LGM precipitation values, which are considerably lower than present-day levels, leading to a greater negative impact on SMB.

It is crucial to highlight that around the LGM, specifically when η approaches 1.2 for NA and η approaches 1.4 for Eurasia, the mean SMB approaches an equilibrium state. When examining the curve in reverse order, it aligns with the observation that during the LGM, the ice sheets ceased growing and initiated a rapid retreat. Given that these simulations are rooted in the LGM state, this outcome suggests that if all settings are set to LGM values, a shift in the temperature pattern towards modern temperature would lead to a rapid reduction in SMB for both NA and Eurasia. Furthermore, Greenland requires a much smaller η to reach the equilibrium state compared to NA and Eurasia.

Varying_P

Figure 4.4 illustrates the mean SMB in response to precipitation changes under intensifying glacial conditions. Notably, precipitation exerts a considerably smaller impact on SMB compared to temperature. The SMB variation due to temperature changes is approximately 50 times greater than that caused by precipitation changes for both NA and Eurasia. In contrast, for Greenland, the SMB variation caused by temperature changes only roughly double that

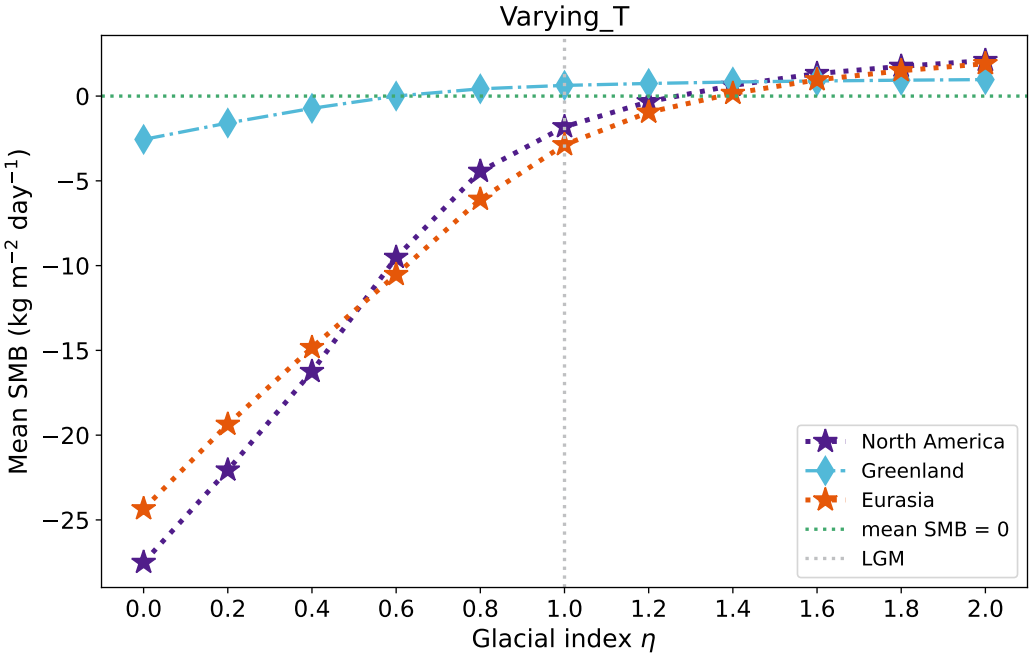

Figure 4.3: Mean SMB evolution in response to increasing glacial severity (higher glacial index), with ***temperature*** *as the sole changing factor.*

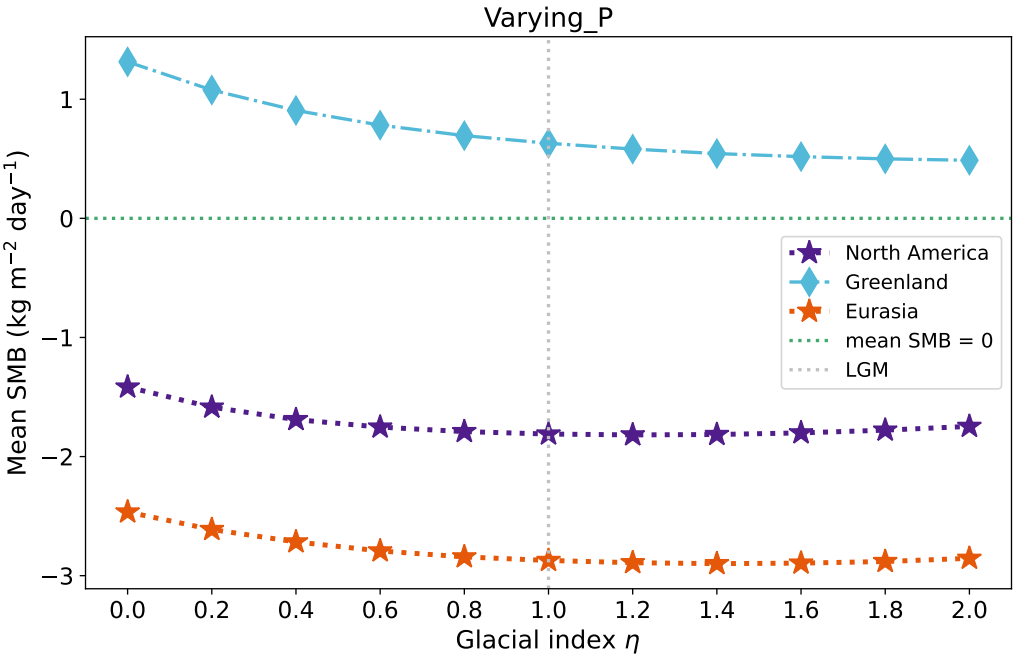

Figure 4.4: Mean SMB evolution in response to increasing glacial severity (higher glacial index), with ***precipitation*** *as the only changing factor.*

caused by precipitation changes.

Furthermore, it is crucial to highlight the complex, non-monotonic pattern in the effect of changing precipitation on SMB for NA and Eurasia, where there is a slight recovery at the end of curve following the initial decline.

Although it is generally believed that many regions in NA and Eurasia experienced arid conditions during the LGM, some areas are thought to have become wetter during this period, such as some parts of western Europe, southwestern Canada and northern America (Figure 3.4). This slight rebound may be influenced by precipitation scaling method employed, but it provides a valuable insight: when the precipitation pattern from present-day to the LGM involves heterogeneous changes, encompassing regions with both increased and decreased precipitation, the predominant effect on the SMB could be less predictable than what the homogeneous change of temperature brings about.

In contrast, for Greenland, there is no recovery at the end of the curve. SMB exhibits a consistent, declining trend, with the slope gradually leveling off. This can be attributed to the fact that the change in precipitation from present-day to the LGM is almost exclusively drying for the majority of Greenland. It is also noteworthy that although the curve for NA closely resembles that for Eurasia, Eurasia experiences a more pronounced negative effect resulting from the Varying_P simulations.

Varying_TP

When we combine variations in temperature and precipitation to explore how these two variables jointly affect SMB, we find that the shape of the curve (Figure 4.5) closely mirrors the one when only temperature is altered (Figure 4.3) for all three regions. This outcome suggests that in terms of the overall evolution trend from present-day to the LGM conditions, temperature has a fundamental influence in altering SMB, while precipitation plays a relatively minor role. This result also aligns with the conclusions drawn from the Varying_T and the Varying_P simulations, which indicates that temperature is roughly 50 times impactful than precipitation for NA and Eurasia, especially when η is relatively small.

The three regions exhibit a similar evolution pattern. Initially, a small increase in glacial temperature and precipitation anomalies leads to a rapid rise in SMB. However, this effect diminishes as η becomes larger, causing the slopes to gradually flatten out.

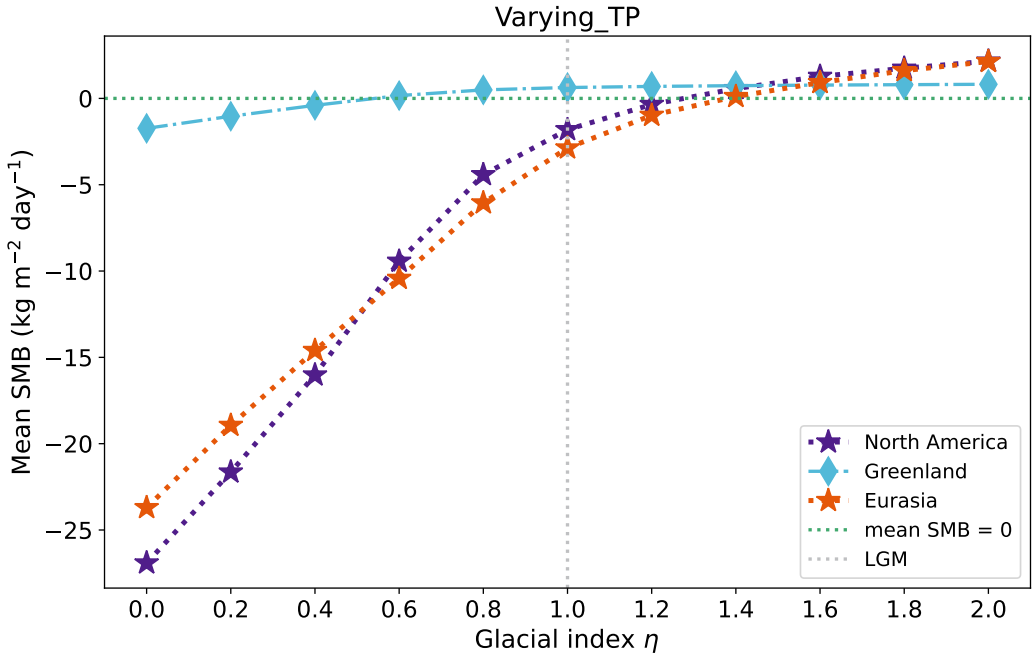

*Figure 4.5: Mean SMB evolution in response to increasing glacial severity (higher glacial index), with **temperature** and **precipitation** as the only changing factors.*

Varying_Z

Topography is another critical factor influencing SMB. It is hypothesized that the presence of continental ice sheets can have a substantial influence on both local and global climate by altering the topography, which, in turn, can either aid their growth or accelerate their demise (Abe-Ouchi et al., 2013; Gallée et al., 1992; Junge et al., 2005; Manabe and Broccoli, 1985; Paillard, 1998). We thus explore the independent impact of topography on SMB.

The connection between topography (elevation) and climate (temperature and precipitation) is primarily governed by lapse rate. In this scenario, we maintain the climate reference height and the climate data constant at LGM values. However, by modifying the actual topography, a discrepancy between the climate reference height and real topography arises. BESSI then calculates the actual climate data by utilizing this elevation difference and the lapse rate. Generally, higher topography leads to colder and drier conditions.

As a result, SMB steadily increases, with the slope gradually leveling off for all three regions. The relatively steep curve in the initial phase may be attributed to the fact that, initially, the positive effect of colder temperature on SMB outweighs the relatively minor negative impact of drier conditions. However, as more regions reach freezing temperatures, further reduction in temperature cannot bring about dramatic positive effects on SMB. Moreover, the

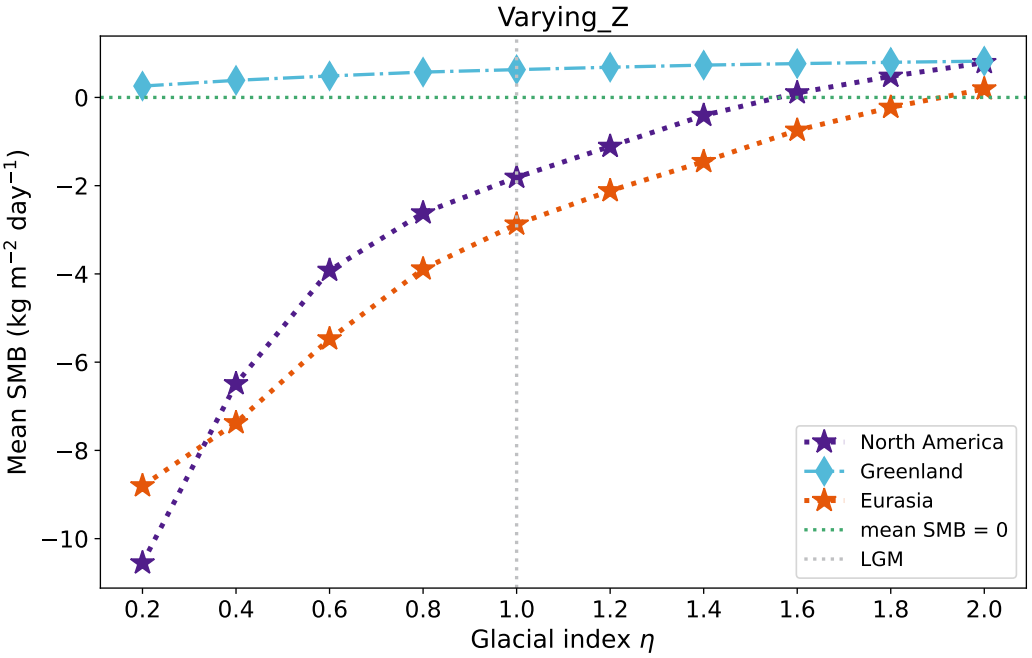

Figure 4.6: Mean SMB evolution in response to increasing glacial severity (higher glacial index), with ***topography*** *as the sole changing factor.*

continued growth in SMB is substantially limited by decreasing precipitation at higher elevation. Consequently, the curves gradually flatten.

It is worth noting that the results from Varying_Z and Varying_T are not identical, with the results from Varying_T showing more pronounced variations. This difference primarily stems from the distinct settings of these two simulations. Varying_Z maintains fixed LGM temperature values, while Varying_T keeps LGM topography constant along with a changeable temperature pattern from present day to 2LGM. As a result, Varying_Z shows a less negative SMB in the initial phase. In the case of Varying_T, the temperatures change represents the actual shift, influenced not only by alternations in topography but also other mechanisms like albedo feedback. The temperature change is thus more pronounced in Varying_T, leading to more significant variations in SMB.

Varying_all

In the Varying_all simulations, none of the key variables are held constant at LGM values. Instead, all the key variables change simultaneously from the current condition towards more severe glacial conditions. This series of simulations closely mirrors what occurs in reality, where all the related variables change concurrently.

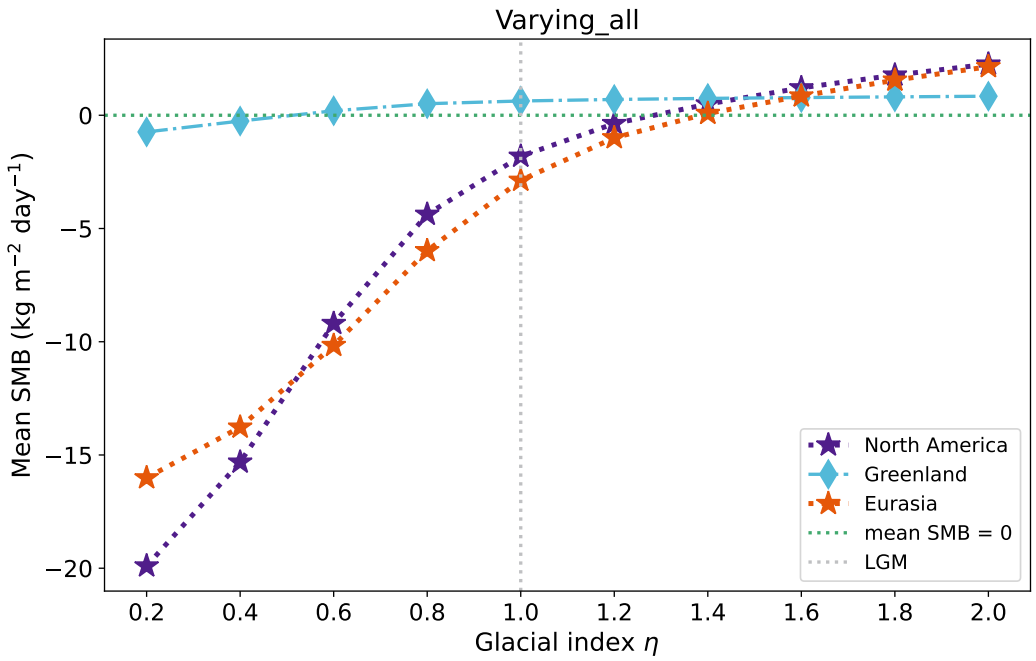

*Figure 4.7: Mean SMB evolution in response to increasing glacial severity (higher glacial index), with **all** relevant variables changing simultaneously, including temperature, precipitation, topography, climate reference height, and sea-level offset.*

Figure 4.7 presents the result of the Varying_all scenario. The curve shapes for NA and Eurasia are largely consistent, with each curve gradually leveling off. In the case of Eurasia, the initial upward trend is notably less pronounced compared to the subsequent segments. This is likely because the cooling effect is not sufficient to lower the temperature to the freezing point in most areas. As a result, the positive impact on SMB is relatively weak. However, with further cooling and as larger portions of land are pushed below the freezing point, SMB increases dramatically. As more and more areas already reach freezing temperatures, the positive effect on SMB brought about by further reduction in temperature diminishes, causing curve's slop to gradually level off.

It is crucial to highlight that around the LGM, specifically when η approaches 1.2 for NA and η approaches 1.4 for Eurasia, the mean SMB approaches an equilibrium state. This might be attributed to the fact that the temperature anomaly between present-day and LGM in Eurasia is smaller than that in North America. Consequently, a larger η is required to introduce a sufficiently positive effect that allows the ice sheet to reach the equilibrium state. This outcome also suggests that when ice sheets are in conditions close to the LGM, a shift towards the current condition could lead to a fast glacial termination.

In comparison to North America and Eurasia, Greenland exhibits smaller variations in

SMB and requires a lower value of η to reach the equilibrium state. This implies during the LGM, large areas of Greenland may still have positive SMB.

4.2.2 Spatial distribution of trends across the Northern Hemisphere

In the previous section, we examined the variations in mean SMB over the three key regions (North America, Eurasia and Greenland). However, assessing mean SMB changes over a large area only provides a rather generalized view, which may not fully capture the intricate developments of SMB in different locations within the vast region. To gain a more detailed and comprehensive understanding of SMB dynamics across the entire domain, we also investigate how SMB responds to the increasingly severe glacial conditions at each individual grid box. Given the substantial number of grid boxes (a total of 313×313), it is impractical to display "SMB-η" figures for every grid box individually. Therefore, we employ polynomial fitting to analyze how SMB varies for individual grid box based on the trends derived from polynomial fitting.

Basic concepts of polynomial fitting

Polynomial fitting is a widely employed mathematical technique for uncovering relationships between variables, frequently applied in regression analysis. In this study, polynomial fitting is applied to determine the best-fitting polynomial that characterizes the "$SMB-\eta$" curve and reveals the underlying trend.

The general form of a polynomial function ($P_{(x)}$) is typically expressed as follows:

$$P_{(x)} = a_n x^n + a_{n-1} x^{n-1} + \ldots + a_2 x^2 + a_1 x + a_0 \tag{4.1}$$

where a_n to a_0 represent coefficients, n signifies the degree of the polynomial, and X denotes the input variable. The primary objective of polynomial fitting is to minimize the discrepancy between $P_{(x)}$ and the actual dataset of another variable Y.

In the context of our study, X is represented by the array of glacial index η, Y is the corresponding array of SMB. This technique enables us to effectively establish the relationship between glacial severity and SMB variations.

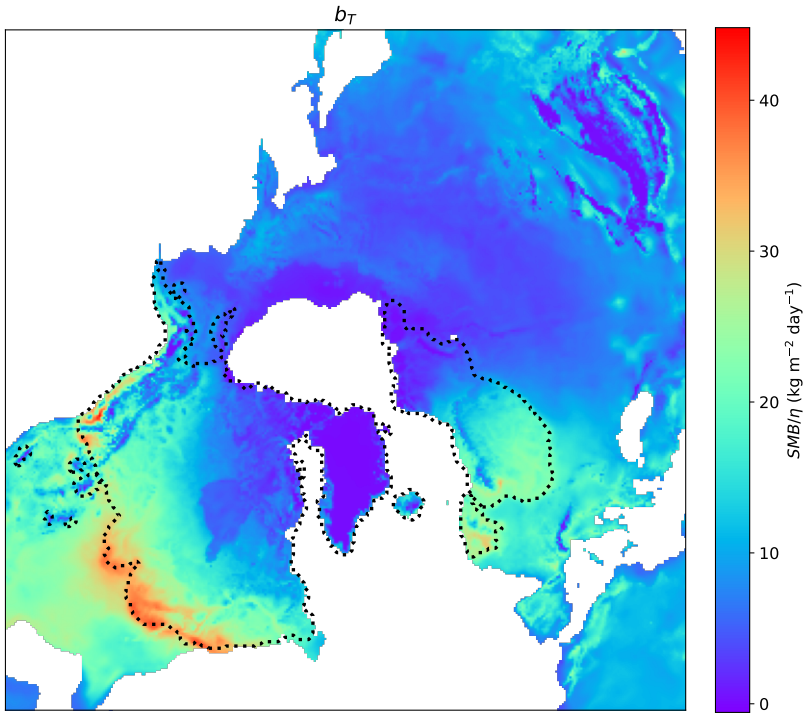

Figure 4.8: Distribution of SMB variation trends when changing temperature as the sole variable. Dotted lines indicate the extent of the ice sheets during the LGM.

Trends in SMB-Temperature relationship

Assuming a linear relationship between the glacial index (η) and the corresponding SMB, we obtain the distribution of linear trends over the whole domain. While this linear assumption may introduce some degrees of underfitting that could potentially affect the precise characterization of the relationship between two variables, it enables us to effectively capture the general trend of how fast SMB changes with the same percentage of increasing glacial severity. Furthermore, it allows us to collectively analyze and visualize the trends of all grid boxes, providing insights into the diverse reactions of different locations.

We begin by examining the relationship between SMB and temperature, using the SMB obtained from Varying_T simulations. Here, b_T represents the linear slope between SMB and glacial index η, indicating the rate of change of SMB for a given level of glacial severity (η). Specifically, a larger b_T suggests a faster rate of SMB change in response to the temperature anomaly introduced by a given level of glacial severity.

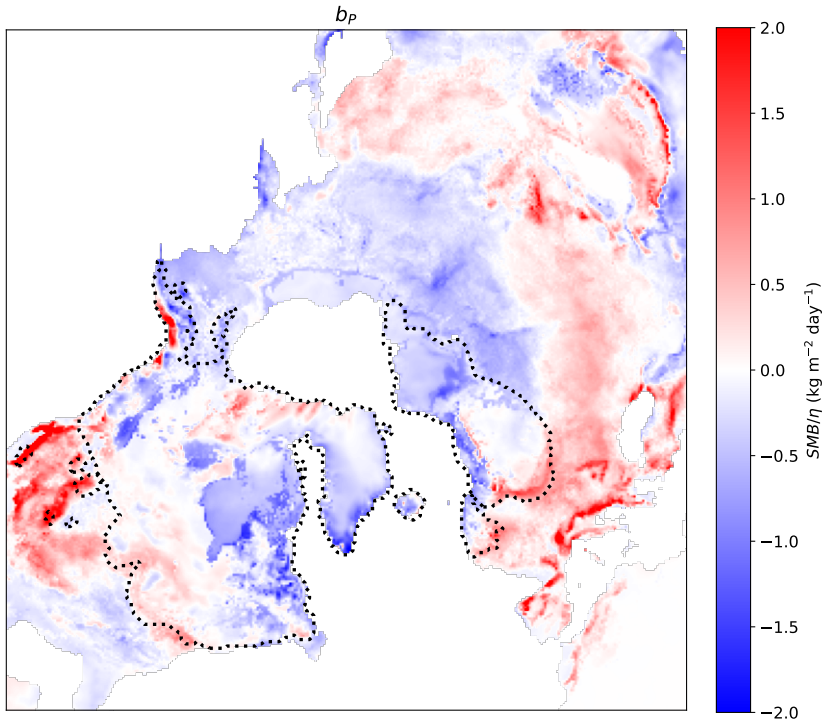

Figure 4.9: Distribution of SMB variation trends when changing precipitation as the sole variable. Dotted lines indicate the extent of the ice sheets during the LGM.

Figure 4.8 illustrates the distribution of linear trends b_T across the entire domain. Notably, SMB changes rapidly along the margin of the North American ice sheet and in certain areas of Western Europe. This may be attributed to the presence of sufficient moisture in these areas, but not low enough temperatures. When a significant cooling effect is introduced (Figure 3.3), a substantial amount of rainfall is converted into snowfall, resulting in a dramatic increase in SMB. Moreover, further reduction in temperature could mitigate the melting in summer seasons for these areas, reinforcing the positive effect on SMB.

In contrast, on Greenland, regions near Hudson Bay and the northeastern part of Eurasia demonstrate relative immunity to temperature changes. This insensitivity may stem from the fact that most of these places are already below the freezing point. Consequently, a further reduction in temperature has minimal impact on further enhancing SMB.

Trends in SMB-Precipitation relationship

Following a similar approach, we investigate the relationship between SMB and precipitation. Here, b_P represents the linear slope between SMB derived from Varying_P simulations and glacial index η. Much like the interpretation of b_T, a large b_P signifies a more rapid SMB variation for a given level of glacial severity.

Figure 4.9 presents the distribution of the linear trends b_P across the whole domain. As mentioned earlier, the precipitation pattern evolves bidirectionally from present-day to the LGM, with some regions becoming drier while others becoming wetter during the LGM (Figure 3.4). Consequently, as glacial severity intensifies, SMB variations also exhibit two distinct patterns. Notably, Figure 4.9 is largely consistent with Figure 3.4, where regions that become significantly wetter undergo a significant increase of SMB, while areas experiencing significant aridity exhibit a substantial decrease in SMB.

It is worth highlighting that Greenland, regions near Hudson Bay and the northeastern part of Eurasia, which show minimal sensitivity to temperature changes, exhibit a remarkable decrease in SMB. This indicates that the aridity introduced by glacial evolution has a substantial impact on SMB in these already cold regions.

4.3 The relative importance of temperature and precipitation anomalies

As mentioned earlier, employing linear fitting to establish the relationship between SMB and η at a broad range may not be a perfect approach, as it can introduce some level of underfitting. The SMB-η figures presented earlier (Figure 4.3 and 4.4) show a clear nonlinearity. Therefore, we refine our analysis by zooming in on specific glacial severity intervals to achieve a more robust linear fit. Our investigation focuses on two distinct glacial severity ranges: the present day (indicated by η ranging from 0 to 0.2 in increments of 0.02) and the LGM (indicated by η ranging from 0.9 to 1.1 in increments of 0.02).

To gain insights into the relative importance of temperature and precipitation for SMB variations within the context of the modern climate and the LGM climate, we conduct two series of simulations, which are Varying_T and Varying_P. This approach allows us to refine our analysis and provide a more accurate assessment of the influence of these two key factors

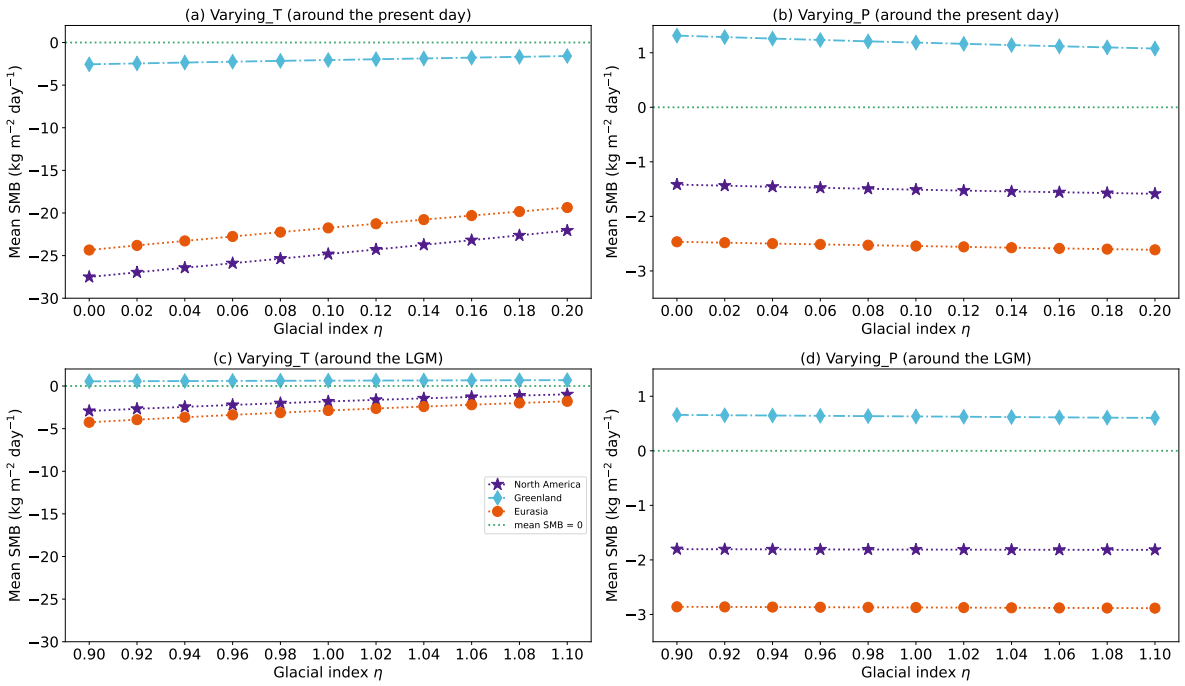

Figure 4.10: Mean SMB evolution in response to increasing glacial severity (higher glacial index). Note that the nearly linear trends in these figures provide a robust basis for employing linear fitting.

on SMB during these specific glacial severity intervals.

Figure 4.10 (a) and (b) illustrate the mean SMB sensitivity to temperature and precipitation when glacial severity approximates the present day, as obtained from Varying_T and Varying_P simulations, respectively. Likewise, Figure 4.10 (c) and (d) present the mean SMB sensitivity to temperature and precipitation for glacial severity around the LGM, obtained from Varying_T and Varying_P, respectively. It is worth emphasizing that the nearly linear trends shown in these figures provide a solid foundation for applying linear fitting.

Additionally, it is notable that in the around present-day scenario, employing the LGM precipitation pattern in combination with modern temperatures (Varying_T) can result in a substantially more negative SMB compared to using LGM temperatures with modern precipitation pattern (Varying_P). While for the around LGM scenario, the range of SMB anomalies in Varying_T and Varying_P is similar, with the variation in SMB derived from Varying_T more pronounced than that from Varying_P.

Subsequently, we compare the linear trends derived from the linear fitting between SMB and the glacial index (η). SMB obtained from the finer sampling of Varying_T and Varying_P are used to determine the linear trends of b_T and b_P, respectively. For a given η, a higher linear slope (b_T or b_P) indicates a more significant variation in SMB. The ratio b_T/b_P thus allows us to assess the relative importance of temperature and precipitation anomalies typical for

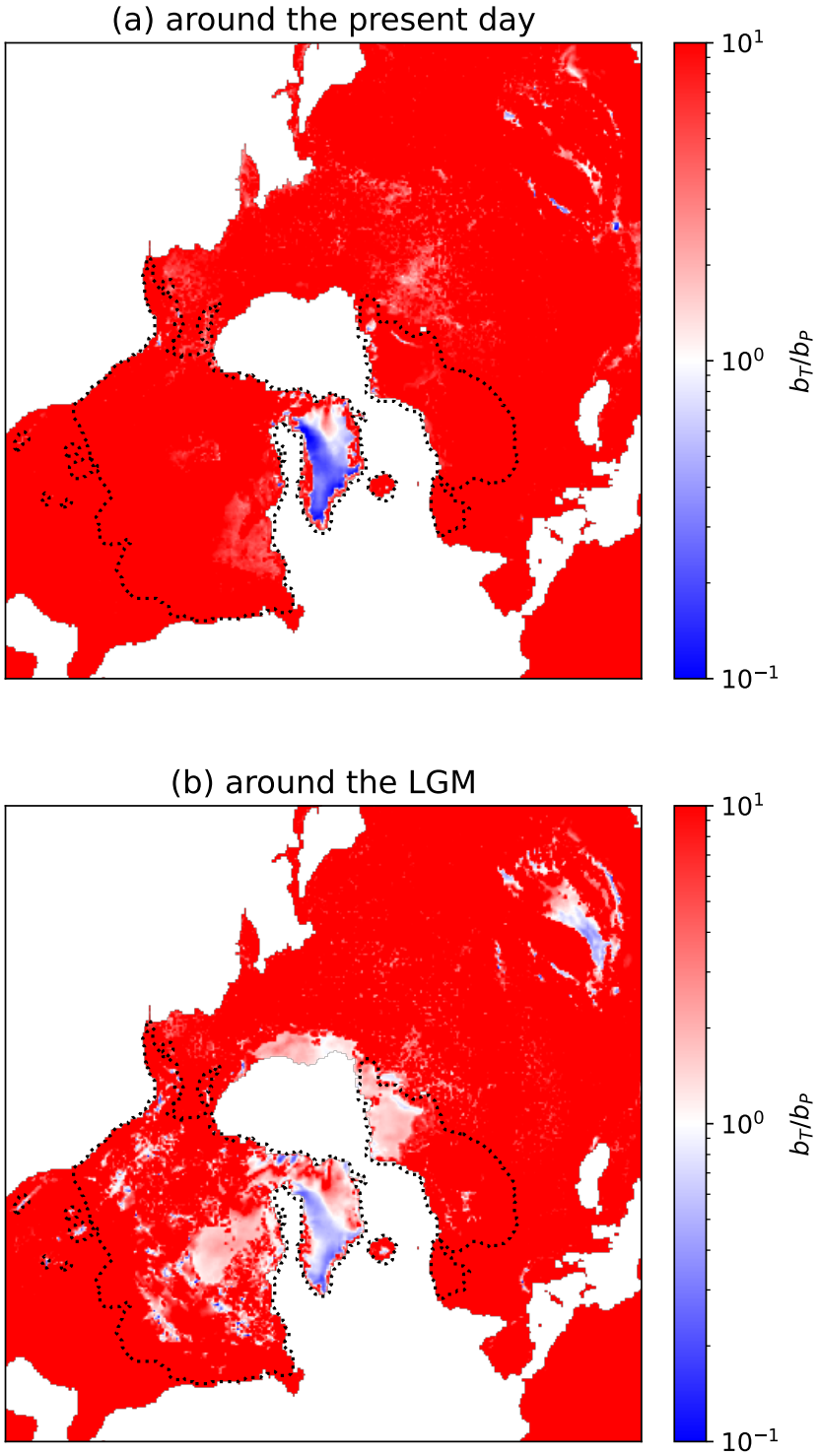

Figure 4.11: A comparison between b_T and b_P across the entire domain for the present day (a) and the LGM (b). Here, b_T (b_P) signifies the linear trends derived from Varying_T (Varying_P) simulations, specifically representing the linear relationships between SMB and the glacial index η. Dotted lines indicate ice sheet extent during the LGM.

glacial/interglacial transitions, thereby identifying the dominant factor driving SMB variations.

To refine our analysis, we zoom in on specific glacial severity intervals, focusing on the periods around the present day and around the LGM. This analysis reveals a relatively high level of consistency for both glacial severity intervals, as illustrated in Figure 4.11. It indicates that SMB variations due to temperature anomalies outweigh those caused by precipitation anomalies for the majority of the investigated areas. Notably, in the southern part of Greenland and specific regions in the Himalaya, precipitation changes have a more pronounced influence for a given glacial severity.

It is important to clarify that this does not imply that regions like northern Greenland are less sensitive to precipitation change. Instead, our primary focus is on the effects brought about by changes that are typical for glacial climate. This means we are particularly interested in how specifically temperature and precipitation anomalies typical of the LGM climate influence SMB. During the transition from present-day to the LGM, there is a much more substantial precipitation change in southern Greenland compared to northern Greenland (Figure 3.4), leading to significantly larger SMB variation in the southern Greenland than in the northern Greenland when same percentage of glacial severity is introduced, which makes b_P larger in southern Greenland.

It is worth noting that in addition to the observed consistency, it is evident that when the glacial severity approaches the LGM, there are larger areas that exhibit lower sensitivity to temperature changes but higher sensitivity to precipitation changes. This is particularly notable in large areas of North America and eastern Eurasia that were covered by ice sheets during the LGM. This suggests that precipitation plays a more important role in the context of the LGM compared to when glacial severity approaches the present day.

To complement this analysis, we perform an additional linear fitting to establish the relationship between actual temperature (precipitation) changes and the corresponding SMB variations for each grid box. Similarly, SMB obtained from the Varying_T and Varying_P simulations are used to determine the linear slope SMB_T and SMB_P, respectively. The biggest difference between b_T (b_P) and SMB_T (SMB_P) is that SMB_T (SMB_P) does not incorporate the glacial index (η) as a variable in the linear fitting. Instead, it uses the actual temperature (precipitation) evolution in response to the intensifying glacial severity to build the relationship with the corresponding SMB for each grid box. Thus, SMB_T reflects the rate of SMB change in response to a 1°C temperature alteration (annual mean) and SMB_P indicates the rate of SMB

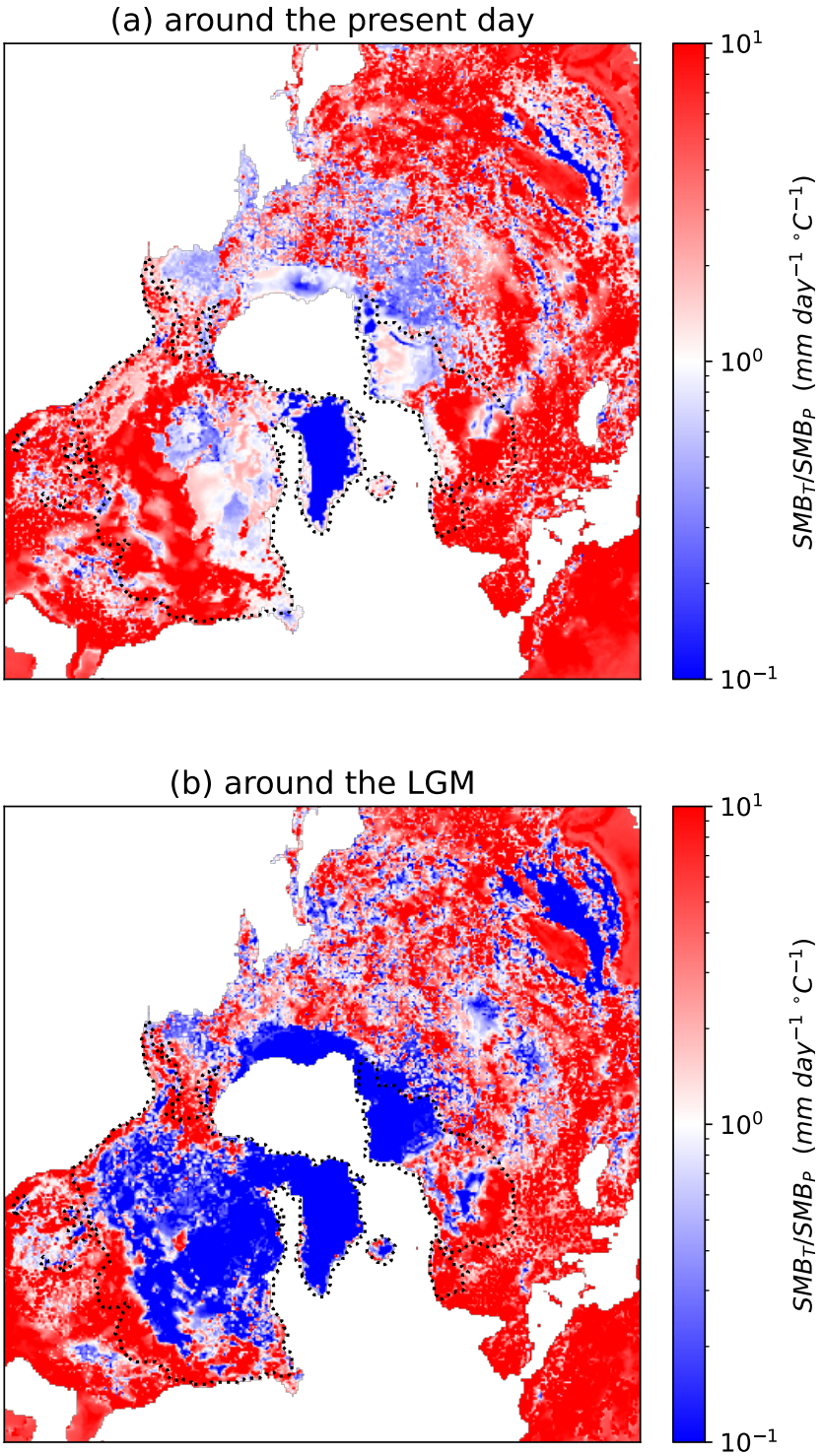

Figure 4.12: A comparison between SMB_T and SMB_P across the entire domain for the present day (a) and the LGM (b). Here, SMB_T (SMB_P) signifies the linear trends derived from Varying_T (Varying_P) simulations, specifically representing the linear relationships between SMB and the actual temperature (precipitation). Specifically, blue area indicates SMB changes more significantly in response to 1 mm/-day precipitation change than 1°C temperature (annual mean), while the red area signifies the opposite. Dotted lines indicate ice sheet extent during the LGM.

change due to a 1 mm/day precipitation change.

Figure 4.12 presents the distribution of the comparison between SMB_T and SMB_P. Specifically, blue area indicates SMB changes more significantly in response to 1 mm/day precipitation change than 1°C temperature (annual mean), while the red area signifies the opposite.

Once more, we observe a clear transition towards increased sensitivity to precipitation changes from the present day to the LGM. Despite some complexity in the patterns, it is evident that regions covered by ice sheets during the LGM, such as North America, Eurasia and Greenland, exhibit a greater sensitivity to a 1 mm/day precipitation change than to a 1°C temperature change within the context of LGM climate.

We also observe notable differences between Figure 4.11 and Figure 4.12, with Figure 4.12 showing more areas possessing a greater sensitivity to precipitation change than to temperature change. Given that the linear trends in Figure 4.11 do not incorporate the actual temperature (precipitation) into the regression, but only compare the SMB variations resulting from a specific η, we may infer that, for a given glacial severity, the magnitude of temperature changes (°C) is higher than the magnitude of precipitation changes (mm/day). This corresponds with the fact that for the typical LGM glacial climate, the temperature anomaly is approximately 30 °C (Figure 3.3), while the precipitation anomaly is about 2 mm/day (Figure 3.4) for the region covered by ice sheets during the LGM.

Chapter 5

Discussion

5.1 Potential dynamics of the three continental ice sheets during the Last Glacial Period

During the Last Glacial Period, it is widely believed that ice sheets in the Northern Hemisphere underwent a long-time growth phase lasting about 90 kyr, followed by a relatively rapid termination phase of about 10 kyr, resulting in a characteristic sawtooth pattern (Broecker and Van Donk, 1970). This 100-kyr cycle corresponds to the dominant frequency observed over the past million years.

However, compared to the relatively well-reconstructed LGM and the subsequent deglaciation, reconstructing the long-time build-up phase of the Last Glacial Period remains largely elusive (Kleman et al., 2010). Several challenges contribute to this knowledge gap (Clark et al., 1993; Kleman et al., 2010). One primary challenge lies in accurately determining the ages of geological records, especially when radiocarbon dating becomes unreliable due to surpassing its age range. Additionally, achieving sufficient resolution for reconstructing the build-up phase is a challenge. This is because landforms and deposits formed during this phase were often overridden by the extensive ice coverage during the LGM. As a result, many geological records that could shed light on this earlier phase have been subjected to destruction and reshaping, leading to a scarcity of available data for reconstructing the build-up phase.

In this study, we utilize a glacial index to explore how the three continental ice sheets (North America, Eurasia and Greenland) respond to the increasing glacial severity, thereby providing the insights into the dynamics of the build-up phase of the Last Glacial Period.

5.1.1 The build-up phase of the Last Glacial Period

During the slow build-up phase that lasted about 90 kyr, there were occasional relatively warmer intervals amidst the prevailing cold trend. It is suggested that the ice volume remained relatively stable during these warmer periods, especially for the North American and Greenland ice sheets (Kleman et al., 2013; Liakka et al., 2016; Mangerud et al., 2023; Stokes et al., 2012). However, recent research indicates that Eurasian ice sheet may have experienced substantial melting during these relatively warmer intervals and could have completely disappeared during Marine Isotope Stage (MIS) 3 (Mangerud et al., 2023). Despite uncertainties regarding the ice sheet behavior during these relatively warm intervals, there is a consensus that throughout the build-up phase towards the LGM, the North American ice sheet experienced a significant expansion (Clark et al., 1993; Kleman et al., 2013), while the Eurasian ice sheet underwent a pronounced westward migration during the same period (Kleman et al., 2013; Svendsen et al., 2004).

In this study, we observe that among the three continental ice sheets, the North American ice sheet exhibits the most pronounced mean SMB sensitivity to the intensifying glacial severity, closely followed by the Eurasian ice sheet. This observation supports the idea that large ice sheets could grow in North America and Eurasia under conditions of significant glacial severity. The Greenland ice sheet, on the other hand, displays smaller variations in SMB. It is worth noting that the change in the total SMB is determined by multiplying the area under investigation by the mean SMB variability over that specific area. Given that North America also possesses the largest area among the three regions, we can infer that the most substantial increase in total ice volume occurred in North America. This observation supports the idea that North America could have experienced a relatively fast and widespread ice sheet growth during the build-up phase. In contrast, the Greenland ice sheet experienced minimal change, assuming that the current conditions are sufficiently similar to the start point of the Last Glacial Period in this region.

It is essential to clarify that in this study, we focus on three fixed regions and do not explicitly consider the temporal dimension. Therefore, we can only provide limited insight into the dynamics of this westward migration for the Eurasian ice sheet. Nevertheless, the high sensitivity of SMB to glacial severity lends support to the notion that a large ice sheet would have grown in that region given sufficiently cold conditions. Moreover, the results of

SMB sensitivity to the key variable changes do not imply the temporal evolution of the build-up phase. Therefore, they do not suggest that during the initial build-up phase, glacial severity gradually intensifies. In reality, considerable ice sheets may have already developed on Eurasia and North America as early as the Marine Isotope Stage (MIS) 5b (85-93 kyr BP) (Kleman et al., 2013; Svendsen et al., 2004), indicating the presence of strong glacial severity during that time. The negative mean SMB values observed over North America and Eurasia can be attributed to the use of expansive land masks that cover large area of these regions. However, the initial glacial growth was primarily concentrated in considerably smaller areas.

While it is suggested that the onset of the Last Glacial Period occurred under climate conditions resembling those of today (Miller and de Vernal, 1992), it is important to acknowledge that the commencement of the Last Glacial Period may not align precisely with the contemporary climate. This study thus only provides a reference for SMB sensitivity. Although some discrepancies may exist, the general trend should be similar. Therefore, the implications obtained from this study remain highly meaningful.

5.1.2 The LGM period

The LGM period is of great scientific interest. During this period, summer insolation levels were suggested to be nearly identical to today, yet large continental ice sheets reached their maximum extent across the Northern Hemisphere. This can be attributed to the strong albedo feedback resulting from the presence of vast ice sheets and lower concentrations of greenhouse gases during that time (Kutzbach et al., 1998; Ruddiman, 2001).

Furthermore, the complex nonlinear response of ice sheets to climate variations likely plays a vital role. It is suggested that the peak cooling of climate did not align precisely with the maximum ice volume (e.g., Oppo et al., 2006). The extensive growth of ice sheets during the LGM may have been facilitated by low summer insolation thousands of years before the LGM. The termination of the ice sheets after the LGM may result from a reversal in insolation, moving towards higher levels. However, the exact reasons for the timing of the termination shortly after the LGM remain largely elusive. Moreover, the stability of large ice sheets and the potential for their collapse remain a subject of ongoing research.

In this study, we have observed that when using climate anomalies between ERA5 (representing present-day climate) and the LGM dataset from CCSM4 to create a typical LGM climate, both the North American and Eurasian ice sheets would experience negative mean

SMB, with values of approximately -1.8 kg/(m^2 day) and -2.9 kg/(m^2 day), respectively. In contrast, Greenland would experience a positive mean SMB of about 0.6 kg/(m^2 day). It is important to note that a larger land mask than Greenland's current size is used in this study for the Greenland ice sheet.

When considering temperature as the sole variable in the glacial severity, North American ice sheets require about 1.2 times the typical LGM glacial severity, while Eurasian ice sheets needs about 1.4 times the typical LGM glacial severity to reach the equilibrium state. Given the more negative SMB in North America in the present day, this result reinforces that the North American ice sheet has the potential to expand fast. It is noteworthy that when considering temperature as one variable in combination with other variables, the results closely mirror the findings when temperature is the sole variable. This similarity is evident when both precipitation and temperature are taken into account as changing factors, as well as when all variables are considered simultaneously.

When precipitation is the exclusive variable under consideration, there is minimal change in SMB for all three regions. Both the North American and Eurasian ice sheets remain in the negative range, while Greenland maintains a positive SMB.

On the other hand, when topography is the only changing factor in determining glacial severity, both the North American and Eurasian ice sheets need more intensified glacial severity to reach an equilibrium state, with approximately 1.6 times and 1.8 times the typical LGM glacial severity, respectively. In contrast, the mean SMB of Greenland remains in the positive range.

In this study, we observe that both the North American and Eurasian ice sheets require more severe glaciation than the typical LGM glacial severity to reach an equilibrium state based on present-day conditions. This finding could signify that the build-up phase requires more intense glacial severity to achieve equilibrium than the reverse process (assuming that during the deglaciation, the LGM represents an equilibrium state). This observation may reflect the complex nonlinear response of ice sheets to climate variations or the presence of hysteresis. Alternatively, it may potentially provide some insights into the fact that the build-up phase takes a longer time to complete, while the termination phase is relatively rapid. However, it is crucial to emphasize that our results are significantly influenced by the size of the investigated area, namely the size of the land-mask; a smaller land-mask could lead to a more positive SMB. Despite some potential bias, the selection of areas covered by the ice sheets during the

LGM is relatively reasonable.

5.2 Sensitivity to climate change at glacial key periods

The Last Glacial Period commenced during a period characterized by a relatively warm climate, much like the present conditions (Kukla et al., 2002; McManus et al., 2002; Miller and de Vernal, 1992). The termination phase, on the other hand, began from the LGM, a time marked by considerably lower temperatures, with the global mean surface air temperature estimated to be about 6°C lower than today and even more pronounced cooling in regions once covered by ice sheets (Tierney et al., 2020). While there is a general consensus that temperature and moisture contents are critical factors in initiating and terminating glaciations (Haug et al., 2005), the precise mechanisms governing glacial inceptions and terminations remain largely elusive. In this study, we explored the relative importance of temperature and precipitation during these key periods of glaciation and deglaciation.

5.2.1 Temperature vs Precipitation

Temperature is a key factor for glacial inception. In our investigation, we observe a significant increase in SMB when colder temperature anomalies are introduced during the initial phase. In contrast, the changes in precipitation resulting from the intensifying glaciation have a minor impact on SMB variations compared to the influence exerted by temperature anomalies during the onset phase. This verifies the importance of cooling for the initiation of glaciation. It is important to highlight that insolation reached its minimum during the onset of the Last Glacial Period (Berger and Loutre, 1991) even though the climate was still relatively warm at that time. This indicates the possibility of a cooling trend at that time.

The critical significance of cooling during the onset of glaciation can be attributed to two key facts (Gildor, 2003): First, it plays a crucial role in transforming rainfall into snowfall, therefore greatly promoting the accumulation. Second, as temperatures drop, it effectively diminishes the process of melting. The combination of increased accumulation and decreased ablation ensures a greater preservation of snow over the years.

In this study, we also observe that as the glacial index (η) rises, the pronounced positive SMB effect resulting from reduced temperature diminishes. This could be attributed to the fact that in regions already sufficiently cold, further reduction in temperature has limited pos-

itive impacts on SMB. Conversely, the significance of precipitation gradually becomes more prominent.

In accordance with the Clausius-Clapeyron equation, atmospheric moisture content increases exponentially with air temperature (Cuffey and Paterson, 2010). Therefore, the extensive growth of ice sheets favors a climate that is relatively warm with an ample supply of moist air. A number of research has demonstrated that ice sheets like Greenland and Antarctica exhibit increased accumulation in response to moderate global warming (Alley et al., 1993; Cuffey and Clow, 1997; Lorius et al., 1979; Van der Veen, 2002), as well as some mountain glaciers, such as the Columbia Ice Field (Luckman, 1988). Our study arrives at a similar conclusion for Greenland, where moisture content plays a dominant role in SMB variations.

Besides the decreased air moisture resulting from colder temperatures, the existing sea ice coverage effectively reduces evaporation from the ocean and redirects storm tracks away from ice sheets (Gildor, 2003; Li and Battisti, 2008). It is hypothesized that ice sheets (glaciers) could withdraw due to the moisture-starved conditions (Gildor and Tziperman, 2000). An extensive sea ice cover is assumed during the LGM (Weinelt et al., 1996), indicating a moisture-deficient environment at that period. The onset of the deglaciation may stem from reduced moisture supply at a global temperature minimum during the LGM. Consequently, the inadequate moisture supply leads to the ice sheets being unable to maintain their original large size, ultimately triggering the termination. The temperature-precipitation feedback further facilitates the onset of deglaciation into a rapid and irreversible retreat. However, our findings primarily do not support the notion that ice sheet termination mainly results from moisture deficiency.

In this study, we note that as glacial severity approaches the LGM ($\eta = 1$), more regions exhibit lower SMB sensitivity to temperature changes but greater sensitivity to precipitation changes. The significance of precipitation becomes increasingly pronounced during the LGM. However, despite this effect, our findings suggest that temperature anomalies maintain a dominant influence over SMB variations. This dominance is evident not only during the onset of glaciation but also under full glacial conditions. It is essential to highlight that this conclusion is based on the SMB variations resulting from the typical climate anomalies between LGM climate and the present-day climate.

However, uncertainties persist regarding the magnitude of climate anomalies during glacial inception and termination. To further elucidate, we broaden our analysis by comparing SMB

variations caused by a 1°C temperature change (annual mean) and a 1 mm/day precipitation. In a climate similar to the modern one, the dominance of temperature variations is evident. However, within the context of the LGM, the impact of precipitation becomes notably stronger. There is greater SMB sensitivity to a 1mm/day precipitation change than to a 1°C temperature change in most areas covered by ice sheets during the LGM.

We thus conclude that the factor of temperature anomalies predominantly governs the onset of glaciation and deglaciation. However, if the magnitude difference between temperature anomalies (°C) and precipitation anomalies (mm/day) is less pronounced, the influence of precipitation could become more prominent.

5.2.2 Temperature-Precipitation feedback

Temperature-precipitation feedback plays a crucial role in regulating local and global climate, emphasizing the interconnected relationship between temperature and precipitation changes.

Elevated temperatures boost evaporation from the Earth's surface and enhance the atmosphere's capacity to hold more moisture. This leads to an increased amount of precipitation being released due to the elevated atmospheric moisture content, either in the form of rainfall or snowfall. Additionally, the higher atmospheric moisture content contributes significantly to a stronger greenhouse effect, trapping more heat. As a result, the increased atmospheric moisture content further amplifies the warming effect.

Moderate warming facilitates the expansion of ice sheets, provided that the rate of accumulation surpasses ablation. However, the threshold for this moderate warming that still permits the growth of ice sheets (glaciers) remains an ongoing topic of research (Gildor, 2003).

5.3 Uncertainties and limitations

In the course of this study, we carefully set up and carry out simulations with the aim of minimizing uncertainties. However, it is crucial to acknowledge that certain inherent uncertainties persist, which may affect the reliability of the findings in this study.

5.3.1 Uncertainties in simulating SMB

One notable uncertainty lies in the simulation of SMB. The accuracy of our simulations depends on various factors, including the accuracy of input data, parameterization, and the representation of physical processes.

Uncertainties in input files

The primary source of uncertainties in the input files is associated with the climate forcing for the LGM. In comparison, the uncertainty in present-day climate forcing is relatively minor. Despite substantial collaborative efforts in projects like the Climate Mapping and Prediction Project (CLIMAP), uncertainties persist in the reconstruction of LGM climate forcing, stemming from aspects such as observational data interpretation. It is important to note that, despite these inherent uncertainties, the LGM climate forcing data used in this study aligns well with global reconstructions and syntheses (Brady et al., 2013).

Another uncertainty in the input files relates to the additional ice thickness during the LGM compared to present-day topography. Reconstructing ice thickness presents inherent challenges, leading to unavoidable uncertainties. However, while there is room for refinements, the ice sheet configuration used in this study is unlikely to significantly deviate from the actual conditions during the LGM (Tarasov and Peltier, 2004).

Uncertainties in BESSI

BESSI has shown robustness to various boundary conditions and is optimized for long-term simulations to assess sensitivity to changes in those conditions (Born et al., 2019). While it balances computational efficiency with a sound representation of physical processes, uncertainties persist like other SMB models.

Variations in parameter values can potentially introduce biases. Notably, factors such as the emissivity of air and coefficient for sensible heat flux exert a substantial influence on the model's performance, both simplified by BESSI with globally uniform single values, potentially leading to biases (Born et al., 2019). Furthermore, uncertainties may exist in the representation of physical processes. For instance, there may be a negative refreezing bias within BESSI (Born et al., 2019). However, a recent study reveals that when calibrating the parameters of BESSI to Regional Atmospheric Climate Model (RACMO), it yields a parameterization

uncertainty negligibly small compared to the uncertainties arising from other factors, such as using different climate models or scenarios (Holube et al., 2022). BESSI also demonstrates good comparability with other SMB models, even the more comprehensive ones (Fettweis et al., 2020).

5.3.2 Uncertainties in interpreting results

Moreover, the interpretation of results is subject to uncertainties originating from several factors.

First, each simulation in our study runs for 500 years, accounting for the time required for the firn cover to achieve both dynamical and thermodynamical stability (Zolles and Born, 2021). Although we employ a back-and-forth climate looping approach involving several years, our primary focus lies on interpreting the results from the final year (i.e., the 500^{th} year of the simulation). This could introduce some bias due to the specific year of climate forcing used for the final year's results. However, given our assumption that typical present-day and LGM conditions have similar climate forcing, this bias should be relatively small. Moreover, any bias stemming from the analysis of a single year would uniformly impact all simulations since the identical year was chosen for each of them.

Second, the results contain the SMB for all 365 days of all grid boxes. But due to the substantial number of SMB data points, we interpret the results using annual mean of SMB, potentially introducing biases by neglecting annual variations.

Third, we use a fixed land-mask to investigate North American, Eurasian and Greenland ice sheets. The choice of land-mask could influence the analysis of results, potentially leading to biases. Nevertheless, selecting a land-mask that corresponds to the areas covered by the ice sheets during the LGM appears to be the most reasonable choice.

While these uncertainties highlight the necessity for further investigations to address and refine our results, we do not expect them to fundamentally alter the robustness of the conclusions drawn.

5.3.3 Limitations

In addition to the inherent uncertainties, this study encounters several limitations.

First, the study lacks explicit consideration of the temporal evolution of climate forcing.

Instead, it only scales the anomalies between the LGM and present-day climates to generate a certain glacial severity, restricting insights into the actual ice sheet evolution. However, this largely depends on the availability of climate data beyond the LGM, emphasizing the need for detailed reconstructions of climate forcing across the Last Glacial Period.

Second, this study exclusively employs a SMB model, without integrating an ice sheet model, thereby neglecting ice-elevation feedback. To achieve a more comprehensive understanding of ice sheet variations, future investigations could integrate ice sheet models to gain a more complete view of ice sheet dynamics in response to climate changes.

Third, we do not account for the downstream influences in this study. It is suggested that changes in the size of the North American ice sheet could have significant impact on the spatial extent of the Eurasian ice sheet, by affecting summer temperatures in Europe and northeastern Siberia (Liakka et al., 2016). Further work could delve deeper into the interaction between these two ice sheets.

Fourth, our analysis relies on one single climate model for the LGM. Given the significance of the LGM climate data in this study, further study could reassess the relative importance of temperature and precipitation by incorporating the LGM climate data from different climate models.

Fifth, we do not explore changes in shortwave or longwave radiation, factors that could influence glaciation and deglaciation (Robinson and Goelzer, 2014). Moreover, these factors are likely to undergo changes in a glacial climate due to variations in cloudiness. Subsequent research could expand this study by incorporating more detailed variables.

Sixth, we solely use a back-and-forth loop for a number of fixed years, neglecting the potentially significant tole of climate variability (inter-annual to decadal variations). A few warm years may prime the SMB for a continued decrease. However, this concern seems to be of minor significance (Zolles and Born, 2022).

It is vital to be aware of these limitations when drawing broader conclusions from this study. However, we do not expect them to fundamentally alter our results.

Chapter 6

Conclusions

In this study, we conduct five series of simulations to explore the relationship between SMB and key variables (temperature, precipitation, and topography). By utilizing the key glacial index factor η, we assess the SMB sensitivity to the changes in these variables as glacial severity increases. Our findings reveal that the SMB variations due to temperature changes is approximately 50 times greater than those caused by precipitation changes, with the changes representing anomalies typical for the glacial-interglacial range. This pattern holds true for both North America and Eurasia, although the positive impact of temperature anomalies diminishes gradually as glacial severity intensifies. When we analyze the combined effects of temperature and precipitation on SMB, we find the results closely mirror those with only temperature altered. This indicates that the dominance of temperature in driving SMB variations across a broad range is evident.

We further analyze specific glacial severity intervals in more detail and quantify the trends of SMB variations due to anomalies in temperature or precipitation. These trends are derived from the linear fitting and provide collective visualization of the diverse reactions from different locations. Clearly, temperature emerges as the dominate factor controlling SMB variations when glacial severity approaches the present day. As glacial severity intensifies, precipitation gains significance, but temperature remains the dominant factor influencing SMB variations, even under full glacial conditions.

Our results suggest that temperature anomalies play a pivotal role in both the onset of glaciation and deglaciation. This challenges a viewpoint suggesting the termination is triggered by moisture deficiency, leading to the inability of large ice sheets to maintain their original size due to insufficient moisture supply.

However, it is important to note that this conclusion is drawn from the anomalies typical for the present-day climate and the LGM climate. If the magnitude difference between temperature anomalies (°C) (annual mean) and precipitation anomalies (mm/day) is less pronounced, the influence of precipitation could become more prominent.

This study also has certain limitations. One significant limitation is the exclusive use of an SMB model without an ice sheet model. To gain a comprehensive understanding of ice sheet dynamics in response to climate change, it is necessary to consider ice variations as well. Further work could incorporate an ice sheet model to reevaluate the relative importance of temperature and precipitation anomalies during key glacial periods to draw a more robust conclusion.

References

Abe-Ouchi, A., Saito, F., Kageyama, M., Braconnot, P., Harrison, S. P., Lambeck, K., Otto-Bliesner, B. L., Peltier, W., Tarasov, L., Peterschmitt, J.-Y., et al. (2015). Ice-sheet configuration in the CMIP5/PMIP3 Last Glacial Maximum experiments. *Geoscientific Model Development*, 8(11):3621–3637. 3.2.2

Abe-Ouchi, A., Saito, F., Kawamura, K., Raymo, M. E., Okuno, J., Takahashi, K., and Blatter, H. (2013). Insolation-driven 100,000-year glacial cycles and hysteresis of ice-sheet volume. *nature*, 500(7461):190–193. 2.4, 2.4.1, 2.4.1, 4.2.1

Alley, R. B., Meese, D., Shuman, C., Gow, A., Taylor, K., Grootes, P., White, J., Ram, M., Waddington, E., Mayewski, P., et al. (1993). Abrupt increase in Greenland snow accumulation at the end of the Younger Dryas event. *Nature*, 362(6420):527–529. 5.2.1

Berger, A. and Loutre, M.-F. (1991). Insolation values for the climate of the last 10 million years. *Quaternary science reviews*, 10(4):297–317. 5.2.1

Bintanja, R., van Oldenborgh, G. J., Drijfhout, S., Wouters, B., and Katsman, C. (2013). Important role for ocean warming and increased ice-shelf melt in Antarctic sea-ice expansion. *Nature Geoscience*, 6(5):376–379. 2.1

Bitz, C. and Battisti, D. (1999). Interannual to decadal variability in climate and the glacier mass balance in Washington, western Canada, and Alaska. *Journal of Climate*, 12(11):3181–3196. 2.2.1

Born, A., Imhof, M. A., and Stocker, T. F. (2019). An efficient surface energy–mass balance model for snow and ice. *The Cryosphere*, 13(5):1529–1546. (document), 1, 2.1, 2.2.2, 3.1.1, 3.1, 3.2, 5.3.1

Box, J., Fettweis, X., Stroeve, J., Tedesco, M., Hall, D., and Steffen, K. (2012). Greenland ice sheet albedo feedback: thermodynamics and atmospheric drivers. *The Cryosphere*, 6(4):821–839. 2.1, 2.2.3

Box, J. E., Cressie, N., Bromwich, D. H., Jung, J.-H., Van Den Broeke, M., Van Angelen, J., Forster, R. R., Miège, C., Mosley-Thompson, E., Vinther, B., et al. (2013). Greenland ice sheet mass balance reconstruction. Part I: Net snow accumulation (1600–2009). *Journal of Climate*, 26(11):3919–3934. 2.2.1

Box, J. E. and Steffen, K. (2001). Sublimation on the Greenland ice sheet from automated weather station observations. *Journal of Geophysical Research: Atmospheres*, 106(D24):33965–33981. 2.2.2

Brady, E. C., Otto-Bliesner, B. L., Kay, J. E., and Rosenbloom, N. (2013). Sensitivity to glacial forcing in the CCSM4. *Journal of Climate*, 26(6):1901–1925. 3.2.1, 5.3.1

Broecker, W. S., Andree, M., Wolfli, W., Oeschger, H., Bonani, G., Kennett, J., and Peteet, D. (1988). The chronology of the last deglaciation: Implications to the cause of the Younger Dryas event. *Paleoceanography*, 3(1):1–19. 2.1

Broecker, W. S. and Van Donk, J. (1970). Insolation changes, ice volumes, and the o18 record in deep-sea cores. *Reviews of Geophysics*, 8(1):169–198. 1, 5.1

Charles, C., Rind, D., Jouzel, J., Koster, R., and Fairbanks, R. (1994). Glacial-interglacial changes in moisture sources for Greenland: Influences on the ice core record of climate. *Science*, 263(5146):508–511. 1

Clark, P., Clague, J., Curry, B. B., Dreimanis, A., Hicock, S., Miller, G., Berger, G., Eyles, N., Lamothe, M., Miller, B., et al. (1993). Initiation and development of the Laurentide and Cordilleran ice sheets following the last interglaciation. *Quaternary Science Reviews*, 12(2):79–114. 2.3.1, 5.1, 5.1.1

Clark, P. U., Dyke, A. S., Shakun, J. D., Carlson, A. E., Clark, J., Wohlfarth, B., Mitrovica, J. X., Hostetler, S. W., and McCabe, A. M. (2009). The last glacial maximum. *science*, 325(5941):710–714. (document), 2.4

Cortijo, E., Duplessy, J., Labeyrie, L., Leclaire, H., Duprat, J., and Van Wearing, T. (1994). Eemian cooling in the Norwegian Sea and North Atlantic ocean preceding continental ice-sheet growth. *Nature*, 372(6505):446–449. 2.4.2

Cuffey, K. M. and Clow, G. D. (1997). Temperature, accumulation, and ice sheet elevation in central Greenland through the last deglacial transition. *Journal of Geophysical Research: Oceans*, 102(C12):26383–26396. 5.2.1

Cuffey, K. M. and Paterson, W. S. B. (2010). *The physics of glaciers*. Academic Press. 2.2, 2.2.1, 2.2.1, 2.2.1, 2.2.1, 2.2.2, 2.2.2, 2.4.2, 5.2.1

Das, I., Bell, R. E., Scambos, T. A., Wolovick, M., Creyts, T. T., Studinger, M., Frearson, N., Nicolas, J. P., Lenaerts, J. T., and Van Den Broeke, M. R. (2013). Influence of persistent wind scour on the surface mass balance of Antarctica. *Nature Geoscience*, 6(5):367–371. 2.2.1

Das, I., Scambos, T. A., Koenig, L. S., Van Den Broeke, M. R., and Lenaerts, J. T. (2015). Extreme wind-ice interaction over Recovery Ice Stream, East Antarctica. *Geophysical Research Letters*, 42(19):8064–8071. 2.2.2

Deblonde, G., Peltier, W., and Hyde, W. (1992). Simulations of continental ice sheet growth over the last glacial-interglacial cycle: experiments with a one level seasonal energy balance model including seasonal ice albedo feedback. *Global and planetary change*, 6(1):37–55. 2.4.3

Dietrich, L., Steen-Larsen, H. C., Wahl, S., Faber, A.-K., and Fettweis, X. (2023). On the importance of the humidity flux for the surface mass balance in the accumulation zone of the Greenland Ice Sheet. *The Cryosphere Discussions*, pages 1–25. 2.2.2

Edwards, T., Fettweis, X., Gagliardini, O., Gillet-Chaulet, F., Goelzer, H., Gregory, J., Hoffman, M., Huybrechts, P., Payne, A., Perego, M., et al. (2013). Effect of uncertainty in surface mass balance–elevation feedback on projections of the future sea level contribution of the Greenland ice sheet–Part 1: Parameterisation. *Cryosphere Discussions*, 7(1). 2.2.3

Ettema, J., van den Broeke, M. R., van Meijgaard, E., van de Berg, W. J., Bamber, J. L., Box, J. E., and Bales, R. C. (2009). Higher surface mass balance of the Greenland ice sheet revealed by high-resolution climate modeling. *Geophysical Research Letters*, 36(12). 1, 2.1

Fettweis, X., Hofer, S., Krebs-Kanzow, U., Amory, C., Aoki, T., Berends, C. J., Born, A., Box, J. E., Delhasse, A., Fujita, K., et al. (2020). GrSMBMIP: intercomparison of the modelled 1980–2012 surface mass balance over the Greenland Ice Sheet. *The Cryosphere*, 14(11):3935–3958. (document), 4.1, 4.2, 5.3.1

Fichefet, T., Poncin, C., Goosse, H., Huybrechts, P., Janssens, I., and Le Treut, H. (2003). Implications of changes in freshwater flux from the Greenland ice sheet for the climate of the 21st century. *Geophysical Research Letters*, 30(17). 2.1

Flatau, P. J., Walko, R. L., and Cotton, W. R. (1992). Polynomial fits to saturation vapor pressure. *Journal of Applied Meteorology (1988-2005)*, pages 1507–1513. 2.2.1

Flint, R. F. (1971). Glacial and Quaternary geology. *(No Title)*. (document), 2.3.1, 2.3

Fyke, J., Eby, M., Mackintosh, A., and Weaver, A. (2014). Impact of climate sensitivity and polar amplification on projections of Greenland Ice Sheet loss. *Climate dynamics*, 43:2249–2260. 2.2.3

Gallée, H., Van Yperselb, J., Fichefet, T., Marsiat, I., Tricot, C., and Berger, A. (1992). Simulation of the last glacial cycle by a coupled, sectorially averaged climate-ice sheet model: 2. Response to insolation and CO2 variations. *Journal of Geophysical Research: Atmospheres*, 97(D14):15713–15740. 2.1, 4.2.1

Gildor, H. (2003). When Earth's freezer door is left ajar. *Eos, Transactions American Geophysical Union*, 84(23):215–215. 1, 5.2.1, 5.2.2

Gildor, H. and Tziperman, E. (2000). Sea ice as the glacial cycles' climate switch: Role of seasonal and orbital forcing. *Paleoceanography*, 15(6):605–615. 5.2.1

Goelzer, H., Robinson, A., Seroussi, H., and Van De Wal, R. S. (2017). Recent progress in Greenland ice sheet modelling. *Current climate change reports*, 3:291–302. 1, 2.1

Haug, G. H., Ganopolski, A., Sigman, D. M., Rosell-Mele, A., Swann, G. E., Tiedemann, R., Jaccard, S. L., Bollmann, J., Maslin, M. A., Leng, M. J., et al. (2005). North Pacific seasonality and the glaciation of North America 2.7 million years ago. *Nature*, 433(7028):821–825. 1, 2.4, 2.4.1, 2.4.2, 5.2

Haug, G. H. and Tiedemann, R. (1998). Effect of the formation of the Isthmus of Panama on Atlantic Ocean thermohaline circulation. *Nature*, 393(6686):673–676. 2.4.2

Hays, J. D., Imbrie, J., and Shackleton, N. J. (1976). Variations in the Earth's Orbit: Pacemaker of the Ice Ages: For 500,000 years, major climatic changes have followed variations in obliquity and precession. *science*, 194(4270):1121–1132. 1, 2.4.1, 2.4.1

Helsen, M. M., Van De Wal, R. S., Reerink, T. J., Bintanja, R., Madsen, M. S., Yang, S., Li, Q., and Zhang, Q. (2017). On the importance of the albedo parameterization for the mass balance of the Greenland ice sheet in EC-Earth. *The Cryosphere*, 11(4):1949–1965. 2.2.3

Hock, R. (2005). Glacier melt: a review of processes and their modelling. *Progress in physical geography*, 29(3):362–391. 2.2.2, 2.2.2

Hoffmann, L., Günther, G., Li, D., Stein, O., Wu, X., Griessbach, S., Heng, Y., Konopka, P., Müller, R., Vogel, B., et al. (2019). From ERA-Interim to ERA5: the considerable impact of ECMWF's next-generation reanalysis on Lagrangian transport simulations. *Atmospheric Chemistry and Physics*, 19(5):3097–3124. 3.2.1

Holland, D. M., Thomas, R. H., De Young, B., Ribergaard, M. H., and Lyberth, B. (2008). Acceleration of Jakobshavn Isbræ triggered by warm subsurface ocean waters. *Nature geoscience*, 1(10):659–664. 2.1

Holube, K. M., Zolles, T., and Born, A. (2022). Sources of uncertainty in Greenland surface mass balance in the 21st century. *The Cryosphere*, 16(1):315–331. 5.3.1

Hughes, A. L., Gyllencreutz, R., Lohne, Ø. S., Mangerud, J., and Svendsen, J. I. (2016). The last Eurasian ice sheets–a chronological database and time-slice reconstruction, DATED-1. *Boreas*, 45(1):1–45. 2.3.2

Huybers, P. (2011). Combined obliquity and precession pacing of late Pleistocene deglaciations. *Nature*, 480(7376):229–232. 1, 2.4.1, 2.4.1

Huybers, P. and Molnar, P. (2007). Tropical cooling and the onset of North American glaciation. *Climate of the Past*, 3(3):549–557. 2.4.3

Imbrie, J., Boyle, E., Clemens, S., Duffy, A., Howard, W., Kukla, G., Kutzbach, J., Martinson, D., McIntyre, A., Mix, A., et al. (1992). On the structure and origin of major glaciation cycles 1. Linear responses to Milankovitch forcing. *Paleoceanography*, 7(6):701–738. 2.4.1

Jóhannesson, T., Sigurdsson, O., Laumann, T., and Kennett, M. (1995). Degree-day glacier mass-balance modelling with applications to glaciers in Iceland, Norway and Greenland. *Journal of Glaciology*, 41(138):345–358. 2.2.1

Johnsen, S., Dansgaard, W., and White, J. (1989). The origin of Arctic precipitation under present and glacial conditions. *Tellus B: Chemical and Physical Meteorology*, 41(4):452–468. 2.3.2

Johnsen, S. J., Clausen, H. B., Dansgaard, W., Gundestrup, N. S., Hammer, C. U., Andersen, U., Andersen, K. K., Hvidberg, C. S., Dahl-Jensen, D., Steffensen, J. P., et al. (1997). The δ18O record along the Greenland Ice Core Project deep ice core and the problem of possible Eemian climatic instability. *Journal of Geophysical Research: Oceans*, 102(C12):26397–26410. (document), 2.5

Johnsen, S. J., Dahl-Jensen, D., Dansgaard, W., and Gundestrup, N. (1995). Greenland palaeotemperatures derived from GRIP bore hole temperature and ice core isotope profiles. *Tellus B: Chemical and Physical Meteorology*, 47(5):624–629. 2.3.2

Junge, M., Blender, R., Fraedrich, K., Gayler, V., Luksch, U., and Lunkeit, F. (2005). A world without Greenland: Impacts on the Northern Hemisphere winter circulation in low- and high-resolution models. *Climate Dynamics*, 24:297–307. 2.1, 4.2.1

Keigwin, L. (1982). Isotopic paleoceanography of the Caribbean and East Pacific: role of Panama uplift in late Neogene time. *Science*, 217(4557):350–353. 2.4.2

Kennett, J. P. and Thunell, R. C. (1975). Global Increase in Quaternary Explosive Volcanism: Volcanic ash in deep-sea sections indicates very high rates of explosive volcanism during the last 2 million years. *Science*, 187(4176):497–503. 2.4.3

Kirkby, J. and Carslaw, K. S. (2006). Variations of galactic cosmic rays and the earth's climate. In *Solar journey: The significance of our galactic environment for the heliosphere and earth*, pages 349–397. Springer. (document), 2.7

Kleman, J., Fastook, J., Ebert, K., Nilsson, J., and Caballero, R. (2013). Pre-LGM Northern Hemisphere ice sheet topography. *Climate of the Past*, 9(5):2365–2378. (document), 2.3.1, 2.1, 5.1.1

Kleman, J., Jansson, K., De Angelis, H., Stroeven, A. P., Hättestrand, C., Alm, G., and Glasser, N. (2010). North American Ice Sheet build-up during the last glacial cycle, 115–21 kyr. *Quaternary Science Reviews*, 29(17-18):2036–2051. 2.3.1, 5.1

Kuhn, T. S. (1987). *Black-body theory and the quantum discontinuity, 1894-1912*. University of Chicago Press. 2.2.2

Kukla, G. J., Bender, M. L., de Beaulieu, J.-L., Bond, G., Broecker, W. S., Cleveringa, P., Gavin, J. E., Herbert, T. D., Imbrie, J., Jouzel, J., et al. (2002). Last interglacial climates. *Quaternary Research*, 58(1):2–13. 1, 5.2

Kutzbach, J., Gallimore, R., Harrison, S., Behling, P., Selin, R., and Laarif, F. (1998). Climate and biome simulations for the past 21,000 years. *Quaternary Science Reviews*, 17(6-7):473–506. 5.1.2

Lambeck, K., Esat, T. M., and Potter, E.-K. (2002). Links between climate and sea levels for the past three million years. *Nature*, 419(6903):199–206. 1

Lenaerts, J. T., Van den Broeke, M., Déry, S., Van Meijgaard, E., Van de Berg, W., Palm, S. P., and Sanz Rodrigo, J. (2012a). Modeling drifting snow in Antarctica with a regional climate model: 1. Methods and model evaluation. *Journal of Geophysical Research: Atmospheres*, 117(D5). 2.2.1, 2.2.2

Lenaerts, J. T., Van den Broeke, M., Van de Berg, W., Van Meijgaard, E., and Kuipers Munneke, P. (2012b). A new, high-resolution surface mass balance map of Antarctica (1979–2010) based on regional atmospheric climate modeling. *Geophysical research letters*, 39(4). 2.2.1, 2.2.2

Li, C. and Battisti, D. S. (2008). Reduced Atlantic storminess during Last Glacial Maximum: Evidence from a coupled climate model. *Journal of Climate*, 21(14):3561–3579. 2.3.3, 5.2.1

Liakka, J., Löfverström, M., and Colleoni, F. (2016). The impact of the North American glacial topography on the evolution of the Eurasian ice sheet over the last glacial cycle. *Climate of the Past*, 12(5):1225–1241. 3.3, 5.1.1, 5.3.3

Lisiecki, L. E. (2010). Links between eccentricity forcing and the 100,000-year glacial cycle. *Nature geoscience*, 3(5):349–352. 1, 2.4.1, 2.4.1

Lorius, C., Merlivat, L., Jouzel, J., and Pourchet, M. (1979). A 30,000-yr isotope climatic record from Antarctic ice. *Nature*, 280(5724):644–648. 5.2.1

Luckman, B. (1988). 8000 year old wood from the Athabasca Glacier, Alberta. *Canadian Journal of Earth Sciences*, 25(1):148–151. 5.2.1

Lunt, D. J., Foster, G. L., Haywood, A. M., and Stone, E. J. (2008). Late Pliocene Greenland glaciation controlled by a decline in atmospheric CO2 levels. *Nature*, 454(7208):1102–1105. 2.4.1, 2.4.1, 2.4.2, 2.4.3

Manabe, S. and Broccoli, A. (1985). The influence of continental ice sheets on the climate of an ice age. *Journal of Geophysical Research: Atmospheres*, 90(D1):2167–2190. 2.1, 4.2.1

Manabe, S. and Stouffer, R. J. (1995). Simulation of abrupt climate change induced by freshwater input to the North Atlantic Ocean. *Nature*, 378(6553):165–167. 2.1

Mangerud, J., Alexanderson, H., Birks, H. H., Paus, A., Perić, Z. M., and Svendsen, J. I. (2023). Did the Eurasian ice sheets melt completely in early Marine Isotope Stage 3? New evidence from Norway and a synthesis for Eurasia. *Quaternary Science Reviews*, 311:108136. 2.3.1, 5.1.1

Maslin, M. A., Li, X., Loutre, M.-F., and Berger, A. (1998). The contribution of orbital forcing to the progressive intensification of Northern Hemisphere glaciation. *Quaternary Science Reviews*, 17(4-5):411–426. 2.4.3

McManus, J. F., Oppo, D. W., Keigwin, L. D., Cullen, J. L., and Bond, G. C. (2002). Thermohaline circulation and prolonged interglacial warmth in the North Atlantic. *Quaternary Research*, 58(1):17–21. 1, 5.2

Miller, G. H. and de Vernal, A. (1992). Will greenhouse warming lead to Northern Hemisphere ice-sheet growth? *Nature*, 355(6357):244–246. 1, 5.1.1, 5.2

Nesje, A., Lie, Ø., and Dahl, S. O. (2000). Is the North Atlantic Oscillation reflected in Scandinavian glacier mass balance records? *Journal of Quaternary Science: Published for the Quaternary Research Association*, 15(6):587–601. 2.2.1

Noël, B., van de Berg, W. J., Machguth, H., Lhermitte, S., Howat, I., Fettweis, X., and Van Den Broeke, M. R. (2016). A daily, 1 km resolution data set of downscaled Greenland ice sheet surface mass balance (1958–2015). *The Cryosphere*, 10(5):2361–2377. 3.1.1

Oerlemans, J. (1980). Model experiments on the 100,000-yr glacial cycle. *Nature*, 287(5781):430–432. 2.4.1, 2.4.3

Öpik, E. J. (1958). Climate and the changing sun. *Scientific American*, 198(6):85–95. 2.4.1

Oppo, D. W., McManus, J. F., and Cullen, J. L. (2006). Evolution and demise of the Last Interglacial warmth in the subpolar North Atlantic. *Quaternary Science Reviews*, 25(23-24):3268–3277. 5.1.2

Paillard, D. (1998). The timing of Pleistocene glaciations from a simple multiple-state climate model. *Nature*, 391(6665):378–381. 2.4, 2.4.1, 2.4.1, 4.2.1

Pollard, D. (1982). A simple ice sheet model yields realistic 100 kyr glacial cycles. *Nature*, 296(5855):334–338. 2.4.3

Pritchard, H., Ligtenberg, S. R., Fricker, H. A., Vaughan, D. G., van den Broeke, M. R., and Padman, L. (2012). Antarctic ice-sheet loss driven by basal melting of ice shelves. *Nature*, 484(7395):502–505. 2.1

Pritchard, M. S., Bush, A. B., and Marshall, S. J. (2008). Neglecting ice-atmosphere interactions underestimates ice sheet melt in millennial-scale deglaciation simulations. *Geophysical Research Letters*, 35(1). 2.1

Rasmussen, L. and Conway, H. (2004). Climate and glacier variability in western North America. *Journal of Climate*, 17(9):1804–1815. 2.2.1, 2.4.2

Rignot, E., Fenty, I., Menemenlis, D., and Xu, Y. (2012). Spreading of warm ocean waters around Greenland as a possible cause for glacier acceleration. *Annals of Glaciology*, 53(60):257–266. 2.1

Rignot, E., Jacobs, S., Mouginot, J., and Scheuchl, B. (2013). Ice-shelf melting around Antarctica. *Science*, 341(6143):266–270. 2.1

Risebrobakken, B., Dokken, T., Otterå, O. H., Jansen, E., Gao, Y., and Drange, H. (2007). Inception of the Northern European ice sheet due to contrasting ocean and insolation forcing. *Quaternary Research*, 67(1):128–135. 1, 2.4.1, 2.4.2

Robinson, A. and Goelzer, H. (2014). The importance of insolation changes for paleo ice sheet modeling. *The Cryosphere*, 8(4):1419–1428. 5.3.3

Ruddiman, W. F. (2001). *Earth's Climate: past and future*. Macmillan. (document), 2.3.2, 2.3.2, 2.6, 2.3.3, 2.4.1, 5.1.2

Ruddiman, W. F. and Kutzbach, J. E. (1989). Forcing of late Cenozoic northern hemisphere climate by plateau uplift in southern Asia and the American West. *Journal of Geophysical Research: Atmospheres*, 94(D15):18409–18427. 2.4.2

Sarnthein, M. (1978). Sand deserts during glacial maximum and climatic optimum. *Nature*, 272(5648):43–46. 2.3.1

Scholz, D. and Hoffmann, D. (2008). 230Th/U-dating of fossil corals and speleothems. *E&G Quaternary Science Journal*, 57(1/2):52–76. 2.3.2

Schoof, C. (2010). Ice-sheet acceleration driven by melt supply variability. *Nature*, 468(7325):803–806. 2.1

Schuler, T. V., Kohler, J., Elagina, N., Hagen, J. O. M., Hodson, A. J., Jania, J. A., Kääb, A. M., Luks, B., Małecki, J., Moholdt, G., et al. (2020). Reconciling Svalbard glacier mass balance. *Frontiers in Earth Science*, page 156. 4.1

Smith, G. I. and Street-Perrott, F. A. (1983). Pluvial lakes of the western United States. *Late-quaternary environments of the United States*, 1:190–212. 2.3.1

Stokes, C. R., Tarasov, L., and Dyke, A. S. (2012). Dynamics of the North American Ice Sheet Complex during its inception and build-up to the Last Glacial Maximum. *Quaternary Science Reviews*, 50:86–104. 5.1.1

Straneo, F., Curry, R., Sutherland, D., Hamilton, G., Cenedese, C., Våge, K., and Stearns, L. (2011). Impact of fjord dynamics and glacial runoff on the circulation near Helheim Glacier, Nat. Geosci., 4, 322–327. 2.1, 2.1

Svendsen, J. I., Alexanderson, H., Astakhov, V. I., Demidov, I., Dowdeswell, J. A., Funder, S., Gataullin, V., Henriksen, M., Hjort, C., Houmark-Nielsen, M., et al. (2004). Late Quaternary ice sheet history of northern Eurasia. *Quaternary Science Reviews*, 23(11-13):1229–1271. 2.3.1, 5.1.1

Tarasov, L. and Peltier, W. R. (2004). A geophysically constrained large ensemble analysis of the deglacial history of the North American ice-sheet complex. *Quaternary Science Reviews*, 23(3-4):359–388. 5.3.1

Tierney, J. E., Zhu, J., King, J., Malevich, S. B., Hakim, G. J., and Poulsen, C. J. (2020). Glacial cooling and climate sensitivity revisited. *Nature*, 584(7822):569–573. (document), 2.3.1, 2.2, 5.2

Van Angelen, J., M. Lenaerts, J., Van den Broeke, M., Fettweis, X., and Van Meijgaard, E. (2013). Rapid loss of firn pore space accelerates 21st century Greenland mass loss. *Geophysical Research Letters*, 40(10):2109–2113. 2.2.1

van den Broeke, M., Bamber, J., Ettema, J., Rignot, E., Schrama, E., van de Berg, W. J., van Meijgaard, E., Velicogna, I., and Wouters, B. (2009). Partitioning recent Greenland mass loss. *science*, 326(5955):984–986. 2.1, 2.2.1, 2.2.3

van den Broeke, M., Box, J., Fettweis, X., Hanna, E., Noël, B., Tedesco, M., van As, D., van de Berg, W. J., and van Kampenhout, L. (2017). Greenland ice sheet surface mass loss: recent developments in observation and modeling. *Current Climate Change Reports*, 3:345–356. 1, 2.2

van den Broeke, M., Smeets, P., Ettema, J., and Munneke, P. K. (2008). Surface radiation balance in the ablation zone of the west Greenland ice sheet. *Journal of geophysical research: Atmospheres*, 113(D13). 2.1, 2.2.2

Van den Broeke, M., Smeets, P., Ettema, J., Van der Veen, C., Van de Wal, R., and Oerlemans, J. (2008). Partitioning of melt energy and meltwater fluxes in the ablation zone of the west Greenland ice sheet. *The Cryosphere*, 2(2):179–189. 2.2.2

Van der Veen, C. (2002). Polar ice sheets and global sea level: how well can we predict the future? *Global and Planetary Change*, 32(2-3):165–194. 5.2.1

van Wessem, J. M., Van De Berg, W. J., Noël, B. P., Van Meijgaard, E., Amory, C., Birnbaum, G., Jakobs, C. L., Krüger, K., Lenaerts, J. T., Lhermitte, S., et al. (2018). Modelling the climate and surface mass balance of polar ice sheets using RACMO2–Part 2: Antarctica (1979–2016). *The Cryosphere*, 12(4):1479–1498. 2.2.1

Vizcaino, M. (2014). Ice sheets as interactive components of Earth System Models: progress and challenges. *Wiley Interdisciplinary Reviews: Climate Change*, 5(4):557–568. 1, 2.1, 2.1, 2.2, 2.2.1, 2.2.3

Vizcaíno, M., Lipscomb, W. H., Sacks, W. J., van Angelen, J. H., Wouters, B., and van den Broeke, M. R. (2013). Greenland surface mass balance as simulated by the Community

Earth System Model. Part I: Model evaluation and 1850–2005 results. *Journal of climate*, 26(20):7793–7812. 2.2.1

Vizcaino, M., Mikolajewicz, U., Ziemen, F., Rodehacke, C. B., Greve, R., and van den Broeke, M. R. (2015). Coupled simulations of Greenland Ice Sheet and climate change up to AD 2300. *Geophysical Research Letters*, 42(10):3927–3935. 2.2.3

Wara, M. W., Ravelo, A. C., and Delaney, M. L. (2005). Permanent El Niño-like conditions during the Pliocene warm period. *Science*, 309(5735):758–761. 2.4.3

Weinelt, M., Sarnthein, M., Pflaumann, U., Schulz, H., Jung, S., and Erlenkeuser, H. (1996). *Ice-free Nordic Seas during the Last Glacial Maximum? Potential sites of deepwater formation*. 5.2.1

Woodard, S. C., Rosenthal, Y., Miller, K. G., Wright, J. D., Chiu, B. K., and Lawrence, K. T. (2014). Antarctic role in Northern Hemisphere glaciation. *Science*, 346(6211):847–851. 2.4.3

Zolles, T. and Born, A. (2021). Sensitivity of the Greenland surface mass and energy balance to uncertainties in key model parameters. *The Cryosphere*, 15(6):2917–2938. 3.1.1, 3.1.2, 5.3.2

Zolles, T. and Born, A. (2022). How does a change in climate variability impact the Greenland ice-sheet surface mass balance? *The Cryosphere Discussions*, pages 1–18. 1, 3.1.1, 3.2.1, 5.3.3